

A model study of air–sea interactions in the Mediterranean Sea

Sergio Castellari^{a,*}, Nadia Pinardi^a, Kevin Leaman^b

^a *IMGA-CNR, Bologna, Italy*

^b *RSMAS, Miami, USA*

Received 1 December 1995; accepted 21 October 1997

Abstract

The surface heat balance is analyzed in all its components to assess the most commonly used heat flux bulk formulas applied to the Mediterranean basin and to provide simulations of better air–sea interaction boundary conditions for Mediterranean OGCMs (Ocean General Circulation Models). A 9-year data set (1980–1988) from 12 hourly NMC atmospheric analysis combined with Reynolds SST and COADS cloud coverage is used. The surface heat balance of the Mediterranean, including the ocean heat advection through the Strait of Gibraltar and the water budget of the basin, is computed using the NMC data at monthly and 12-hourly frequency. The 12-hourly NMC data yield the correct heat loss in the basin. This analysis identifies a set of heat flux bulk formulas (‘the calibrated set’) which represent best the heat balance of the Mediterranean Basin with our available data sets. The calibrated set of bulk formulas, used as heat flux boundary condition for the OGCM, is capable to improve the representation of the water masses in the Mediterranean basin and to reduce the model climatic drift. © 1998 Elsevier Science B.V. All rights reserved.

Keywords: heat; flux; air–sea interaction

1. Introduction

The Mediterranean Basin (Fig. 1) is driven by intense buoyancy fluxes (high latent and sensible heat fluxes), that must be understood if we are to incorporate thermodynamic forcing at the air–sea interface of ocean general circulation models (OGCMs) (Malanotte-Rizzoli and Bergamasco, 1991; Roussenov et al., 1995; Zavatarelli and Mellor, 1995; Castellari, 1996; Pinardi et al., 1997).

In the Mediterranean Sea, the general circulation is composed by sub-basin scale gyres and intense coastal boundary currents (Millot, 1991; Robinson et

al., 1991) and three main water masses are formed. The Levantine Intermediate Water (LIW) can be formed in most of the Northern Levantine Basin (Ozsoy et al., 1989) and frequently in the Rhodes area (Lascaratos et al., 1993). The eastern deep water, called Eastern Mediterranean Deep Water (EMDW), is formed in the Adriatic Sea (Ovchinnikov et al., 1987; Artegiani et al., 1997). The western deep water, called Western Mediterranean Deep Water (WMDW), is formed in the Gulf of Lions (Leaman and Schott, 1991; Schott et al., 1993). Also in the Eastern Mediterranean the Aegean Water (called Cretean Intermediate Water) is formed in the Aegean Sea and can be found between 500 and 1200 m (Schlitzer et al., 1991). All these waters are formed during extreme wintertime conditions characterized

* Corresponding author.

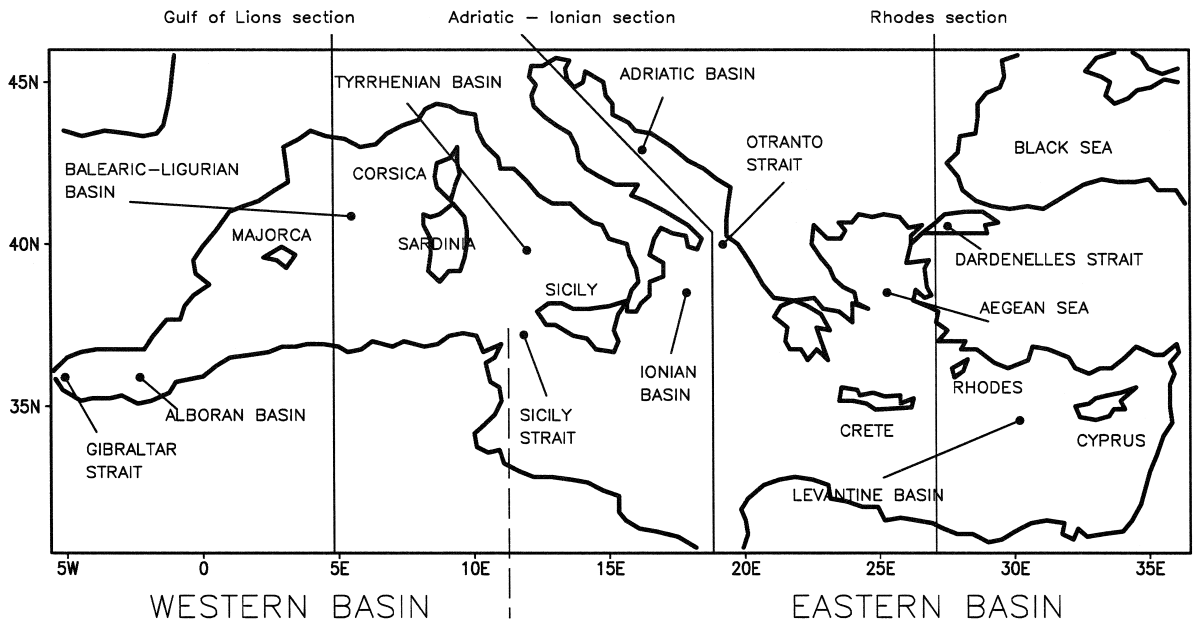


Fig. 1. Mediterranean basin nomenclature with the locations of the three sections.

by strong surface cooling and evaporation due to outbreaks of cold and dry air.

Furthermore, the Mediterranean basin offers the opportunity of calibrating the air–sea physics parameterizations in order to give a known steady-state surface heat balance. The ‘Mediterranean heat budget closure problem’ can be stated as follows: the advective heat flux through the Strait of Gibraltar (considering Black Sea heat flux to be negligible) has an annual average of $7 \pm 3 \text{ W/m}^2$ (Lacombe et al., 1964; Boyum, 1967; Bethoux, 1979; Bunker et al., 1982) or $5.2 \pm 1.3 \text{ W/m}^2$ in the more recent study of Macdonald et al. (1994). At steady-state, the advective heat flux through Gibraltar should be compensated by a net heat loss at the sea surface of the same amplitude. Furthermore, using the terrestrial branch of the water cycle it is possible to estimate the evaporation E from which the basin averaged latent heat flux can be found. Thus the ‘Mediterranean heat budget closure problem’ tries to calculate a total heat budget of approximately 7 W/m^2 keeping a value for E as computed from water budget considerations.

The ocean surface heat budget (Q_T) can be computed as the downward solar radiation flux (Q_S) minus the net longwave radiation flux (Q_B) minus

the sensible heat flux (Q_H) and the latent heat flux (Q_E). (Here the fluxes Q_B , Q_H and Q_E are positive for energy gained by the atmosphere). In Table 1, we show a synthesis of previous results for Q_T and its components in the Mediterranean Sea.

Garrett et al. (1993) estimated the heat budget with the COADS (Slutz et al., 1985) data set for the period 1946–1988. The COADS included the ‘observed’ monthly means of the standard meteorological variables (wind components, cloudiness, specific humidity, sea surface and air temperature) and the monthly averaged products of some variables (sea–air temperature difference and wind magnitude, saturations and wind magnitude). Thus, sensible and

Table 1
Mediterranean long term mean heat budget: the left hand column indicates the authors of different Q_T estimates

Authors	Q_S	Q_B	Q_H	Q_E	Q_T
Bethoux (1979)	195	68	13	120	–6
Bunker et al. (1982)-(1)	202	68	13	101	20
Bunker et al. (1982)-(2)	202	68	11	130	–7
May (1986)	193	68	11	112	2
Garrett et al. (1993)	202	67	7	99	29
Gilman and Garrett (1994)	183	77	7	99	0

latent heat fluxes are partially computed from instantaneous values, while net longwave radiation fluxes and the turbulence exchange coefficients are computed from monthly mean data. The budget net value ($+29 \text{ W/m}^2$) was not compatible with the Gibraltar constraint. To reduce the budget they suggested a possible correction (a constant adjustment factor) to the solar radiation term (-18%) or to the latent and sensible heat terms ($+33\%$). Finally, Gilman and Garrett (1994) modified extensively the results of Garrett et al. (1993). They reduced the solar radiation by approximately 9% by removing an error due to an incorrect parameterization of the solar radiation at very low cloud values (2%), by using daily climatological estimates of cloudiness (4%) and by accounting for the attenuation of incoming solar radiation by atmospheric aerosols (3%). This correction for aerosol variability was compared with ground measurements in two locations, and it agreed with one. They also increased the net longwave radiation by about 15% by using a regression formula based on preliminary measurements over the Tyrrhenian Sea (Bignami et al., 1991). With all these modifications, Gilman and Garrett (1994) reached a zero value for Q_T .

Here we will study the question of Mediterranean heat budget closure by using the conventional bulk formulations of air–sea physics but utilizing a modern atmospheric data set with high temporal resolution. Our data set is composed of 12-hourly operational analyses at 1000 hPa for a period of 9 years (from January 1980 to December 1988). This is one of the primary data set used to force realistic simulations of the ocean circulation (Rosati and Miyakoda, 1988; Heburn, 1994; Roussenov et al., 1995; Castellari, 1996; Pinardi et al., 1997). However, no studies have been done in order to see if a realistic heat budget can be estimated with bulk formulas and operational analysis fields. On the other hand the operational analyses are an important data set in order to drive a OGCM and study the ocean response to external forcing.

We will first show that the atmospheric operational data sets can give consistent solutions to the ‘Mediterranean heat budget closure problem’ (identifying a set of air–sea physics bulk formulations) and then we will show the sensitivity of the OGCM to different sets of air–sea physics parameterizations.

We use the OGCM implemented on the Mediterranean Sea by Roussenov et al. (1995) and force with climatological parameters extracted from our data sets. We then analyze the sensitivity of the water mass structure to different sets of air–sea physics parameterizations. In Section 2, we describe the meteorological and sea surface data sets used in the calculations; in Section 3, the different air–sea interaction physics parameterizations and the water budget estimates; in Section 4, we show the heat budget, interannual variability and error analysis; in Section 5, we present the usage of the calibrated set of air–sea interaction physics on the OGCM and Section 6 offers the conclusions.

2. Features of the meteorological and oceanographic data sets

Basic fields are the zonal and meridional components of the wind speed (u , v), air temperature (T_A), relative humidity (r), sea surface temperature (T_S) and cloud cover (C) (Castellari et al., 1990; Castellari and Pinardi, 1992). The first four parameters are taken from NMC 1000 hPa analyses (National Meteorological Center now NCEP, Washington, DC) at spectral resolution R30, twice daily (0Z and 12Z), for the period January 1980–December 1988. The data were mapped on a $1^\circ \times 1^\circ$ grid. The forecast model used daily SST analyses computed with two-day time window of in situ and satellite data for the period 1980–1985 and daily SST analyses computed with 15-day time window of in situ and satellite data for the period 1986–1988 as described by Reynolds (1988). Thus a word of caution should be said in the interpretation of the results, because of the mismatch between our computations and the SST used by the model. In our case, sea surface temperature data are obtained from global monthly mean CAC analyses (Climate Analysis Center, Washington, DC) obtained with a combination of ship opportunities and satellite data (Reynolds, 1982). The SST (or T_S) data were available in two data sets: one for the period 1970–1981 on a $2^\circ \times 2^\circ$ grid, the other for the period 1982–1988 on a $1^\circ \times 1^\circ$ grid. Cloud cover data are taken from COADS (Slutz et al., 1985) as mapped by Oort and Pan (1985) on a $1^\circ \times 1^\circ$ grid. We do not use cloud data from the NMC forecast model be-

cause they are thought to be unreliable. The data sets, twice-daily NMC data, are denoted in the following as the Daily Data Set (DDS).

From the twice daily NMC data we calculated a Monthly mean Data Set (MDS). The u , v monthly averages are made by calculating directions and amplitudes of the wind vectors and averaging each separately (scalar average). Compared to a vector average of the wind speed components, this averaging procedure has been shown (Hanawa and Toba, 1987) to give more reasonable flux estimates (less bias compared to instantaneous estimates). The usage of atmospheric parameters at 1000 hPa instead of 10 m was decided on the basis of their utilization to force OGCM (Rosati and Miyakoda, 1988). This choice has also been prompted by the concern that the surface analysis fields would be too much dependent on the particular boundary layer parameterization in use at any given moment in the NMC assimilation schemes. Thus we choose to use a slightly inconsistent data set to evaluate bulk formulas, since 1000 hPa is higher than 10 m on average in the Mediterranean, but we will demonstrate the validity of this choice on the basis of the correct OGCM response. Below we briefly describe the atmospheric data sets and their seasonal and interannual variabilities for the period 1980–1988.

Winter winds over the Mediterranean basin are westerly with an important meridional component due to the Mistral in the Balearic–Ligurian Sea. The variability of basin average wind speed amplitudes and directions is larger in winter than in summer due to the strong northerly Mistral component (Fig. 2). The summer wind regime shows less variability and is dominated by the northerly component of the Etesian winds in the Eastern Mediterranean.

In general, the NMC wind velocity data overestimate the dominant westerly component of the wind stress over the Mediterranean basin with respect to the Hellermann and Rosenstein (1983) and May (1986) data sets (not shown here). Time series of overall Mediterranean monthly averages (Fig. 3) clearly show the Mistral signal every winter (December–February) with a maximum in January 1981 (10.2 m/s), and the secondary Etesian maximum almost every summer. The anomalously strong January 1981 Mistral, along with the T_A minimum ($\sim 10^\circ\text{C}$) in the same month, produces the T_S mini-

mum (14°C) in February of the same year. The strong January 1981 Mistral has also been found by Heburn (1994) in his analysis of the interannual variability of an atmospheric ECMWF (European Centre for Medium-Range Weather Forecasts) data set used to force a Mediterranean model. The NMC data show a trend of increasing summer air temperatures since 1984, reaching about 34°C for the summers of 1987 and 1988 (Fig. 3). An other warm summer is that of 1982, following the coolest summer in 1981. The summer T_S and T_A peaks tend to track one another except for the anomalous values in 1987 and 1988. The coldest winter (January 1981) has a minimum T_A of around 10.6°C ; the next coldest winter value (11.8°C) occurs in March 1987. In general T_S is warmer than T_A by $\sim 2^\circ\text{C}$ in winter, while during the summer $T_A \sim T_S + 3^\circ\text{C}$, except for the anomalous summers in 1987 and 1988 ($T_A \sim T_S + 8^\circ\text{C}$).

The NMC 1000 hPa relative humidity signal shows low values, with a surface average of 61% and an anomalous minimum of 43% in April 1981. The cloud coverage data realistically represent sky conditions over the Mediterranean, with an average of 0.4 and a strong seasonal cycle (large values in winter and smaller in summer).

In the period 1980–1988 the coldest year is 1981, which is characterized by both the coldest winter (with the strongest winds and less saturated air over the sea) and the coolest summer; and the warmest year is 1988 (mild winter and hot summer). In general, time series of all data show clear seasonal periodicities with a dominant yearly period but with large interannual variabilities. A comparison between NMC 12-hourly data and those of Leaman and Schott (1991) (a combination of measurements and model results in the Gulf of Lions for the period 20 January to 10 March 1987) shows agreement with the NMC air temperature and wind velocity data, with T_A having almost the same average value (9°C) and maxima and minima on the same days (Castellari, 1996). However, NMC relative humidity shows smaller values with a range of about 50%–100%, compared to 62%–100% of Leaman and Schott (1991).

The quality of model generated data (such as NMC) and the impact of changes in the forecast system on the resulting fields are important consider-

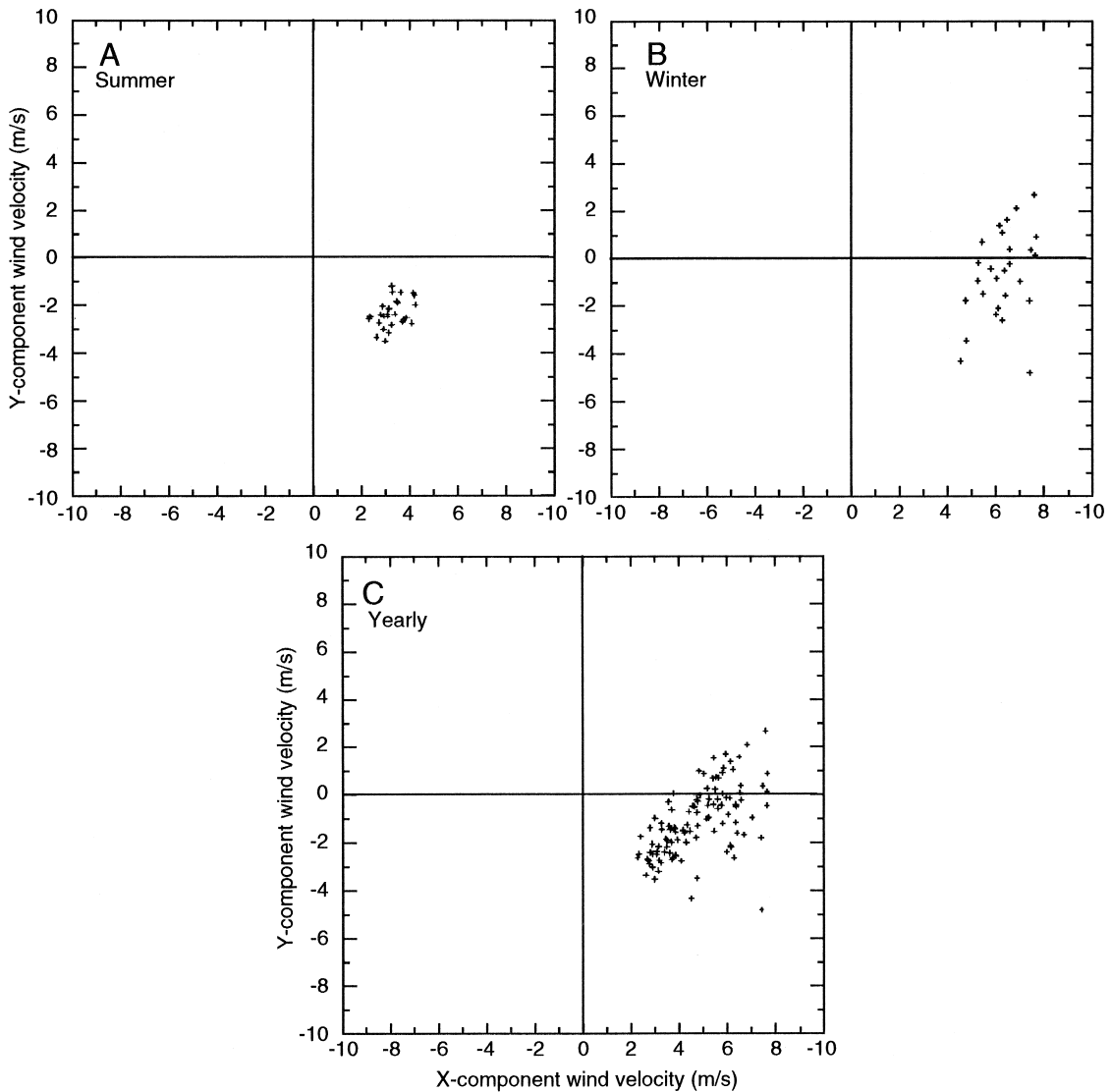


Fig. 2. Scatter plot of the Mediterranean basin surface averages of u and v for: all summers (A), all winters (B) and all year (C).

ations. Trenberth and Olson (1988a,b) evaluated the NMC global analyses in comparison to ECMWF. In general the NMC quality is very poor in the tropics and Southern Hemisphere and the NMC has more missing and bad data than ECMWF. The biggest impacts on the 1980–1988 NMC analyses probably came from changes in the physics of convective processes in the forecast model, which affected the 1000 hPa winds and relative humidity over Antarctica and Africa (in particular the Sahara region).

Over the Mediterranean area, no specific comparison ECMWF vs. NMC was carried out. We believe that the significant increment in air temperature shown in the years after 1986, despite possible biases, is not a consequence of the change in parameterizations in the operational schemes. Santoleri et al. (1994) have studied the seasonal and interannual variability of the Western Mediterranean basin through the analysis of satellite T_s for the period 1981–1990. They have found an increase in T_s from 1984 to 1990 with the

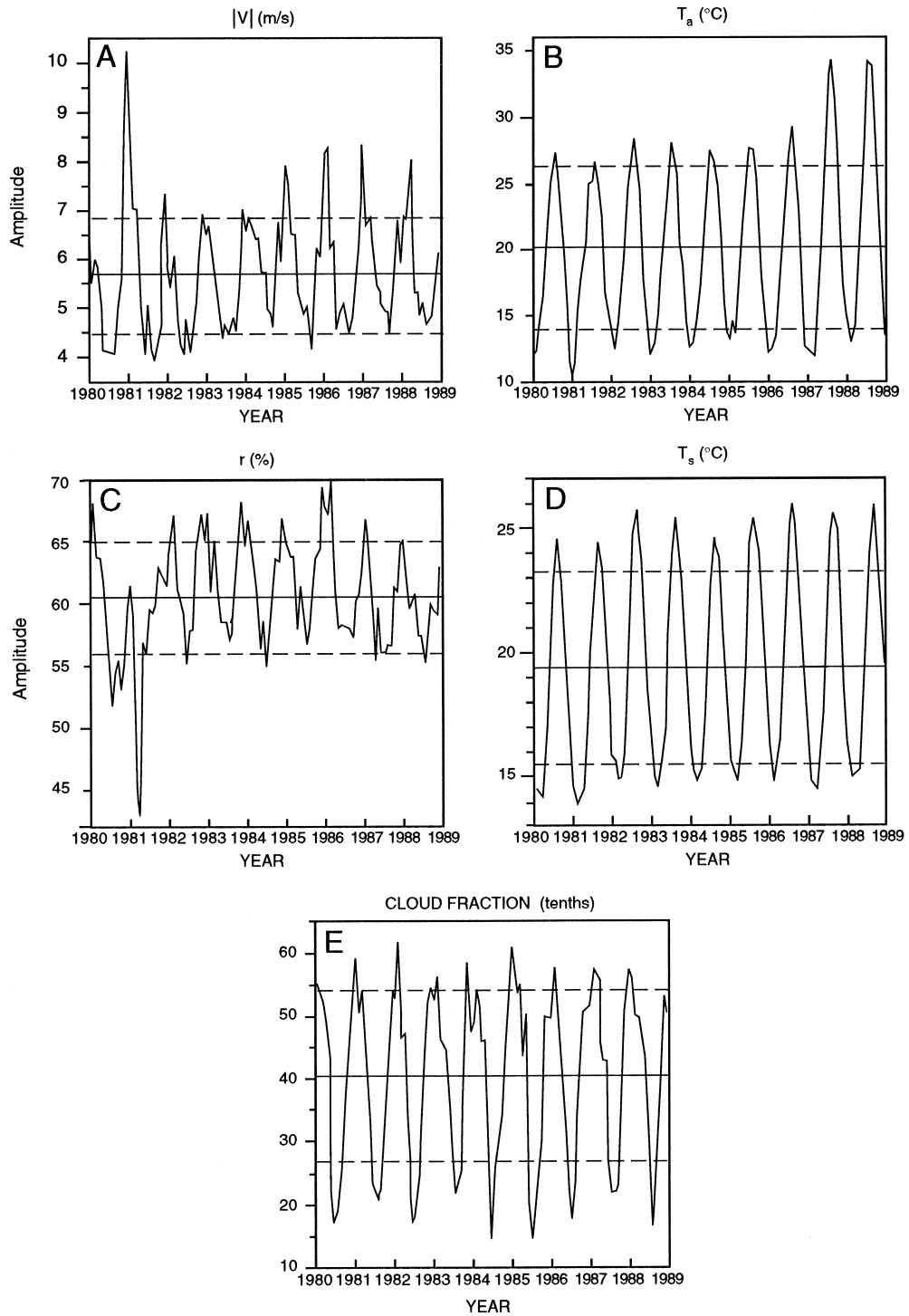


Fig. 3. Time series of surface averaged monthly NMC $|\vec{V}|$ (A), T_A (B), r (C), Reynolds T_S (D) and COADS cloud fraction (E) for the period January 1980–December 1988. The interannual mean and ± 1 standard deviation lines are also indicated.

warmest summer in 1987, which corresponds to the increase in NMC T_A detected in this study.

3. Air–sea interaction physics

3.1. Solar radiation flux

The solar radiation flux is the largest term in the heat budget of the ocean. A number of parameters are needed for its calculation, including the total radiation reaching the ocean surface under clear sky Q_{TOT} (direct and diffuse), the transmissivity of the atmosphere τ and the cloudiness C .

In most studies (Reed, 1977; Simpson and Paulson, 1979; Weare et al., 1981; Isemer and Hasse, 1987; Garrett et al., 1993; Gilman and Garrett, 1994), Q_{TOT} has been calculated through the ‘Smithsonian Formula’ derived by Seckel and Beaudry (1973) as a function of latitude and time. This formula compares well with coastal and oceanic clear-sky insolation observations made by Reed (1975) (weighted mean difference of -2% for 322 days) and by Reed and Halpern (1975) (positive daily bias of 30% for 10 days).

Since these comparisons are based on short records at particular locations, we have chosen instead to use present-day astronomical formulations for Q_{TOT} (Hsiung, 1986; Rosati and Miyakoda, 1988), that we think could be more precise in latitude and longitude. In this case the total solar radiation reaching the ocean surface under clear sky is represented by its components Q_{DIR} (direct solar radiation) and Q_{DIFF} (downward diffuse sky radiation):

$$Q_{TOT} = Q_{DIR} + Q_{DIFF} = Q_0 \tau^{\sec z} + \frac{[(1 - A_a)Q_0 - Q_0 \tau^{\sec z}]}{2} \quad (1)$$

where Q_0 is the solar radiation at the top of the atmosphere, τ (0.7) is the atmospheric transmission coefficient attenuating the direct radiation, A_a (0.09) is the water vapor plus ozone absorption and z is the zenith angle. The term Q_0 has been calculated as a function of latitude, longitude and time using astronomical parameters taken from the *Smithsonian Meteorological Tables* (List, 1958).

An empirical relationship describes the effect of clouds and albedo on the solar radiation reaching the ocean surface. By analyzing coastal observations Reed (1977) proposed a formula suitable for the tropics and high latitudes. Another formula is from Lumb (1964), which is more comprehensive since it includes different cloud types. Simpson and Paulson (1979) and Dobson and Smith (1988) found that both the *Reed* and the *Lumb* relations are in close agreement with observations. Instead, Schiano et al. (1993) found that both *Lumb* and *Reed* formulas underestimate solar radiation under cloudy conditions (*Lumb* formula is closer to the experimental data than *Reed*'s). They suggested that the bulk formulas do not account for the extra downward radiation reflected by the cloud edges. Originally the *Reed* formula was intended to be used with daily estimates of C , but it can be used quite correctly with monthly estimates of cloudiness because the cloud reduction term is linearly dependent on the cloud cover C . Isemer et al. (1989) and Garrett et al. (1993) used the *Reed* formula with monthly averaged cloud cover data. Gilman and Garrett (1994) found a reduction of 4% in their climatological Q_S value by using daily climatological cloud values (U.S. Navy, 1955), but this result is not definitive because the comparison was done with different types of cloud cover data sets.

Therefore we have decided to use the *Reed* formula, because we use monthly cloud cover data without specification of cloud type.

The *Reed* formula is:

$$Q_S = Q_{TOT}(1 - 0.62C + 0.0019\beta)(1 - \alpha) \quad (2)$$

where C is the fractional cloud cover (tenths), β is the solar noon altitude in degrees, and α is the ocean surface albedo. The albedo is computed as a function of the sun zenith angle for each grid point from Payne (1972). This formula, according to Reed (1977), could overestimate the Q_S values for low cloudiness values. Thus we considered $Q_S = Q_{TOT}$ if $C < 0.3$.

We decided to keep the value of 0.7 for the atmospheric transmission coefficient, and we do not consider any possible effect of aerosols particles affecting the solar radiation flux. Gilman and Garrett (1994) estimated the possible effect of aerosol parti-

cles (anthropogenic sulfates and mineral aerosols) and applied a simple correction to the estimation of the solar radiation which was reduced by 3%. This possible correction (applied to a solar radiation flux on the sea surface) was compared only with two ground measurements (Malta and Cyprus) and agreed with the one made in Cyprus. This comparison cannot be considered definitive since this measurement was made at 162 m above the sea level as pointed out from Schiano (1996). Also Gilman and Garrett (1994) decided to neglect the effects of aerosols particles on the net longwave radiation flux, but this can be as well important according to Bethoux and Gentili (1994).

3.2. Net outgoing longwave radiation flux

The choice of the appropriate formula for net outgoing longwave radiation flux (Q_B) presents the same uncertainty as the choice for solar radiation. We compare several available formulations (Table 2), noticing that the $e_{\text{sat}}(T_A)$ term has been computed through a polynomial approximation as a function of temperature by Lowe (1977). We apply the *Brunt–Berliand* formula in two versions: the first as used by Rosati and Miyakoda (1988) in the forcing of their GFDL model (Eq. (1) in Table 2), the second following Budyko (1974) (Eq. (3) in Table 2). We also apply another version (known as the *Berliand–Berliand* formula—Eq. (4) in Table 2), which has

been used by Oberhuber (1988) in his heat budget calculation with the COADS data set. Our *Efimova* formula is the same version used by Isemer et al. (1989) in their study on the Atlantic ocean. The *May* formula (May, 1986) is a modified *Berliand–Berliand* formula with a nonlinear cloud term multiplying the whole expression and without the ocean emissivity factor. In all these formulations the cloud term (linear or not) and its coefficient play a crucial role in determining the values of Q_B . The cloud factor could depend on latitude, as suggested by Reed (1977) and by *Berliand* (Budyko, 1974), or could depend on the cloud type, as suggested by Laevastu (1967). Bunker et al. (1982), with the purpose of correcting a possible bias arising from the usage of surface data, developed a method of construction of seasonal charts of Q_B (using the Elsasser radiation diagrams) for three different cases: a complete cover of low clouds, a complete cover of medium and high clouds and a clear sky. By applying this method Bunker et al. (1982) increased their previous value for Q_B over the Mediterranean Sea from 52 W/m² to 68 W/m². Instead in this study we consider the cloud coefficient as a constant, since we have C available as monthly means of observed average clouds with no specification of cloud type.

Recent radiation measurements (Bignami et al., 1995) in the Western Mediterranean Sea during different seasons showed that the difference between the empirical bulk formulas listed above and the

Table 2
Different bulk formulas for the net outgoing longwave radiation flux

Author	Formula
1) Brunt–Berliand-(a) ^a	$Q_B = \epsilon\sigma T_S^4(0.39 - 0.05\sqrt{e_A})(1 - 0.8C) + 4\epsilon\sigma T_S^3(T_S - T_A)$
2) Efimova ^b	$Q_B = \epsilon\sigma T_A^4(0.254 - 0.00495e_A)(1 - 0.65C) + 4\epsilon\sigma T_A^3(T_S - T_A)$
3) Brunt–Berliand-(b) ^b	$Q_B = \epsilon\sigma T_A^4(0.39 - 0.058\sqrt{e_A})(1 - 0.65C) + 4\epsilon\sigma T_A^3(T_S - T_A)$
4) Berliand–Berliand ^c	$Q_B = \epsilon\sigma T_A^4(0.39 - 0.05\sqrt{e_A})(1 - 0.65C) + 4\epsilon\sigma T_A^3(T_S - T_A)$
5) May ^d	$Q_B = [\sigma T_A^4(0.4 - 0.05\sqrt{e_A}) + 4\sigma T_A^3(T_S - T_A)](1 - 0.75C^{3.4})$
6) Bignami et al. ^e	$Q_B = \epsilon\sigma T_S^4 - [\sigma T_A^4(0.653 + 0.00535e_A)](1 + 0.1762C^2)$

ϵ = Ocean emissivity; σ = Stefan–Boltzman constant; $e_A = re_{\text{sat}}(T_A)$ = atmospheric vapor pressure; $e_{\text{sat}}(T_A)$ = atmospheric saturation vapor pressure; T_A = air temperature; T_S = sea surface temperature; C = cloud coverage.

^aFrom the work of Rosati and Miyakoda (1988).

^bFrom the work of Budyko (1974).

^cFrom the work of Berliand and Berliand (1952).

^dFrom the work of May (1986).

^eFrom the work of Bignami et al. (1995).

experimental data can be as high as $\sim 30 \text{ W/m}^2$. They also described a new formula for Q_B , which was computed with a statistical regression method on the experimental data. We list this new formula in Eq. (6) of Table 2.

3.3. Sensible and latent heat fluxes

The sensible (Q_H) and latent (Q_E) heat fluxes are parameterized through classical bulk aerodynamic formulas as:

$$Q_H = \rho_A C_p C_H |\vec{V}| (T_S - T_A) \quad (3)$$

$$Q_E = \rho_A L_E C_E |\vec{V}| \left[(e_{\text{sat}}(T_S) - re_{\text{sat}}(T_A)) \frac{0.622}{p_A} \right. \\ \left. = \rho_A L_E C_E |\vec{V}| [q_S - q_A] \right] \quad (4)$$

where $\rho_A = \rho_A(p, T_A, \tau)$ is the density of moist air, C_p is the specific heat capacity, C_H and C_E are turbulent exchange coefficients, L_E is the latent heat of vaporization, $|\vec{V}|$ is the wind speed, $e_{\text{sat}}(T_S)$ and $e_{\text{sat}}(T_A)$ are the saturation vapor pressures at temperatures T_S and T_A , q_S is the saturation specific humidity of air with temperature T_S , q_A is the specific humidity of the air, and p_A is the surface air pressure (fixed at 1000 hPa). L_E has been calculated as a function of temperature from the work of Gill (1982).

From the many parameterization schemes that have been proposed to describe the variability of C_H and C_E using parameters such as $|\vec{V}|$, T_S , T_A and the virtual temperature T_v , we have chosen four (Table 3), which all have been applied to the Mediterranean Sea previously. We note that the evaporation E can be estimated from Eq. (4).

Table 3
Different schemes for the turbulent coefficients C_H and C_E

Scheme	Formulation
1) Neutral ^a	$C_E = C_H = 1.1 \times 10^{-3}$
2) Neutral Budyko ^b	$C_E = C_H = 2.1 \times 10^{-3}$
3) Kondo ^c	$C_E = C_E(\vec{V} , T_S - T_A)$, $C_H = C_H(\vec{V} , T_S - T_A)$
4) Smith ^d	$C_E = C_H(\vec{V} , T_S - T_v)$, $C_H = C_E / 1.2$

^aFrom the work of Rosati and Miyakoda (1988).

^bFrom the work of Budyko (1963).

^cFrom the work of Kondo (1975).

^dFrom the work of Smith (1989).

Table 4

Climatological estimates of the different terms for the Terrestrial Branch of the Mediterranean water budget

P (m/yr)	G (m/yr)	R (m/yr)	E (m/yr)	Q_E (W/m^2)
0.55–0.70	0.56–0.66	0.21	1.32–1.57	103–122

3.4. Evaporation and water budget

The net evaporation budget E can also be estimated from the terrestrial branch of the water cycle:

$$E = P + G + R. \quad (5)$$

where P is the precipitation, G is the Gibraltar exchange and R is the runoff from rivers and Black Sea. For all the terms we take the most recent values in order to describe maximum/minimum values of E . For the precipitation we use minimum/maximum values from the work of Jaeger (1976) (0.55 m/yr) and Legates and Willmott (1990) (0.70 m/yr). For the Gibraltar exchange we use the range of values from the works of Bryden and Kinder (1991a,b) (0.56–0.66 m/yr) and for the runoff we use the adjusted value from the work of Rohling and Bryden (1992) (0.21 m/yr).

As shown in Table 4, the evaporation range calculated from Eq. (5) is 1.32–1.57 m/yr, which correspond to a range of Q_E of about 103–122 W/m^2 . This range of values of E from the terrestrial branch of the Mediterranean water cycle is larger than the range of values (1.21–1.36 m/yr) from the aerological branch (Gilman and Garrett, 1994); in particular the maximum value is higher. Despite the fact that Mediterranean water budget calculations present considerable uncertainty in all terms, we will use these estimates to constrain maximum values of Q_E in the heat budget calculations.

4. Heat budget components over the Mediterranean Sea

4.1. The long term mean heat budget

We now compute the components of the surface heat budget as a function of different bulk formulas. One formulation for Q_S , six bulk formulas for Q_B ,

and four schemes for Q_H and Q_E are used to estimate the climatological mean of each heat budget term and Q_T as the residual.

Our calibrated set of bulk formulas has been judged on the basis of the ‘closure’ conditions.

(1) The ability to produce the required annual heat budget of $-7 \pm 3 \text{ W/m}^2$ to compensate for the average gain of heat through the Strait of Gibraltar.

(2) The ability to maintain the evaporative budget within the range of Table 4 computed from the terrestrial branch of the water cycle.

We evaluate the 9-year mean of the different heat budget terms using the different formulations applied to both MDS and DDS data (Table 5). Q_S has always a climatological value of 202 W/m^2 , which is consistent with past values by Bunker et al. (1982) and Garrett et al. (1993) (see Table 1).

The formulas for Q_B in Table 5 give values ranging from 44 W/m^2 to 84 W/m^2 , where the larger values seem to be more related to the nonlinearity of the cloud term in the formulas rather than to

the powers of T_S or T_A or to the MDS, DDS data sets. Using the most recent data of Bignami et al. (1995) we obtain the maximum value of 84 W/m^2 .

Using the different formulations for latent and sensible heat flux in Table 5 we see that major changes occur due to the use of DDS and MDS data sets. It is interesting to notice that the *Smith* scheme is always biased toward low values because of its underestimation of Q_H and Q_E with high and moderate winds (Jones et al., 1993; Gulev, 1994). An interesting change between DDS and MDS data occurs in the Q_H term: 225% and 66.7% increase for the *Kondo* (1975) and *Smith* (1989) schemes. Latent heat fluxes show increased values with the *Kondo* and *Smith* schemes which are smaller than the corresponding sensible heat fluxes (the new Q_E values with the *Kondo* and *Smith* schemes have respectively increased only of 6.1% and 12.7%), respectively.

The possible final Q_T values are listed in Table 6. For MDS Q_T ranges from 7 W/m^2 to 67 W/m^2 (Table 6). The best solution to the closure problem of the Mediterranean heat budget is found in experiments 2 ($Q_T = 18 \text{ W/m}^2$) and 3 ($Q_T = 7 \text{ W/m}^2$), which use both the *Kondo* scheme for Q_H and Q_E , but the *Berliand–Berliand* and *May* formulas for Q_B in experiments 2 and 3, respectively.

In the case of the DDS data set we can reach negative Q_T values. In fact, the large increase of Q_H with DDS data allows us to close successfully the heat budget problem. Experiment 6 of Table 6 shows that with the *May* formula and the *Kondo* scheme we get a value for Q_T of -11 W/m^2 . The significant increase of Q_H with DDS is accompanied by a much smaller percentage increase of Q_E (only 6.1%), which results in an evaporation rate of 1.57 m/yr , which is within the acceptable values from the terrestrial branch of the water cycle. Another interesting result comes from the usage of Bignami et al. (1995) formula for Q_B , which gives along with *Kondo* scheme (experiment 7 of Table 6) the largest heat loss for the Mediterranean Basin (-17 W/m^2). We believe this is a reasonable solution for the heat budget closure problem, but the only way to judge the difference would be to see the effects on the ocean water column temperatures in detail. We consider experiment 6 in Table 6 to represent the calibrated air–sea interaction physics.

Table 5

Climatological values of the different heat budget components estimated with the different formulations and data sets

Parameterizations	Q_S	Q_B	Q_H	Q_E
Reed	202	–	–	–
Brunt–Berliand-(a) (MDS)	–	48	–	–
Efimova (MDS)	–	47	–	–
Brunt–Berliand-(b) (MDS)	–	44	–	–
Berliand–Berliand (MDS)	–	65	–	–
May (MDS)	–	76	–	–
Neutral Scheme (MDS)	–	–	–4	91
Neutral Budyko Scheme (MDS)	–	–	–6	174
Kondo Scheme (MDS)	–	–	4	115
Smith (MDS)	–	–	6	79
Brunt–Berliand (a) (DDS)	–	51	–	–
Efimova (DDS)	–	73	–	–
Brunt–Berliand-(b) (DDS)	–	46	–	–
Berliand–Berliand (DDS)	–	67	–	–
May (DDS)	–	78	–	–
Bignami et al. (DDS)	–	84	–	–
Neutral Scheme (DDS)	–	–	2	90
Neutral Budyko Scheme (DDS)	–	–	4	170
Kondo Scheme (DDS)	–	–	13	122
Smith Scheme (DDS)	–	–	10	89

Q_S = solar radiation flux.

Q_B = net outgoing longwave radiation flux.

Q_H = sensible heat flux.

Q_E = latent heat flux.

Q_T = heat budget.

Table 6

Long term mean surface integrals of the heat fluxes estimated with different sets of bulk formulations to test how close the long term mean Q_T is to $-7 \pm 3 \text{ W/m}^2$

Test	Q_S	Q_B	Q_H	Q_E	Q_T
1) MDS	202	48	-4	91	67
2) MDS	202	65	4	115	18
3) MDS	202	76	4	115	7
4) DDS	202	67	13	122	0
5) DDS	202	73	13	122	-6
6) DDS	202	78	13	122	-11
7) DDS	202	84	13	122	-17

Only the most significant tests are shown.

The left hand column indicates the set of formulas used (1 through 7) and the meteorological data set used.

Test 1: Q_H , Q_E from neutral scheme as in Table 3; Q_B from Brunt–Berliand formula as in Table 2; MDS data set.

Test 2: Q_H , Q_E from Kondo scheme as in Table 3; Q_B from Berliand–Berliand formula as in Table 2; MDS data set.

Test 3: Q_H , Q_E from Kondo scheme as in Table 3; Q_B from May formula as in Table 2; MDS data set.

Test 4: Q_H , Q_E from Kondo scheme as in Table 3; Q_B from Berliand–Berliand formula as in Table 2; DDS data set.

Test 5: Q_H , Q_E from Kondo scheme as in Table 3; Q_B from Efimova formula as in Table 2; DDS data set.

Test 6: Q_H , Q_E from Kondo scheme as in Table 3; Q_B from May formula as in Table 2; DDS data set.

Test 7: Q_H , Q_E from Kondo scheme as in Table 3; Q_B from Bignami et al. formula as in Table 2; DDS data set.

4.2. Interannual variability

We now examine the interannual variability of the heat budget components. All daily components of the heat budget calculated with the best formulations (experiment 6 in Table 6) have been monthly averaged over the basin.

The time series of Q_S (Fig. 4) is dominated by a strong seasonal cycle with a small interannual signal, since the only interannually varying factor is the cloud term. The term Q_B (Fig. 5) ranges from 54 W/m^2 to 109 W/m^2 for the 1980–1986 period with a maximum in December 1986, and it shows large negative anomalies in the summers of 1987 and 1988 when Q_B reaches a minimum value of 9 W/m^2 .

Q_H is smaller than either Q_B or Q_E . It changes sign around April and September (Fig. 5C) and ranges from -23 to 85 W/m^2 with strong interannual variability: there are three large maxima in

January 1981 (85 W/m^2), December 1986 (67 W/m^2) and January 1986 (59 W/m^2). These maxima are related to strong Mistral winds and air temperature minima in the same period (Fig. 3). A minimum in July 1988 of -23 W/m^2 is also present and is related to the maximum in T_A .

Q_E in general reproduces the same features of Q_H (Fig. 5E), and has its maximum in January 1981 (279 W/m^2) and two pronounced minima in August 1987 (22 W/m^2) and in July 1988 (20 W/m^2).

The Q_T time series (Fig. 5G) shows a smooth signal dominated by Q_S and interannually modulated by Q_E . The minima are in January 1981 (-387 W/m^2) and December 1986 (-334 W/m^2), while the maxima are in July 1987 (317 W/m^2) and July 1988 (341 W/m^2).

We have not estimated the heat storage in the Mediterranean Basin to check consistency with the interannual signal of Q_T . Garrett et al. (1993) estimated the heat storage of the Mediterranean and found that the interannual variability of their estimated fluxes could not be compatible with the variability of the heat storage. Further analysis is required on this important issue, which will not be done here.

In Fig. 5 we also compare experiment 6 to experiment 3 of Table 6 in order to show visually the differences between DDS and MDS data sets. We find that for Q_B (Fig. 5B) the largest differences occur during summer and especially those of 1981

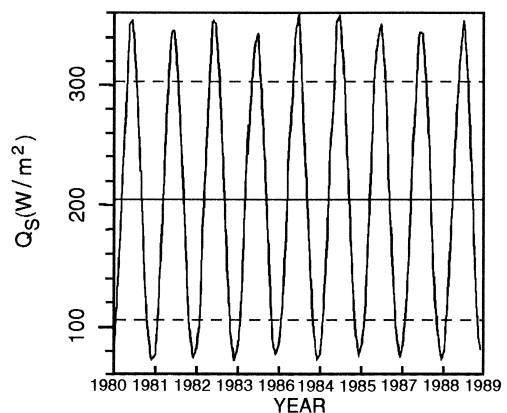
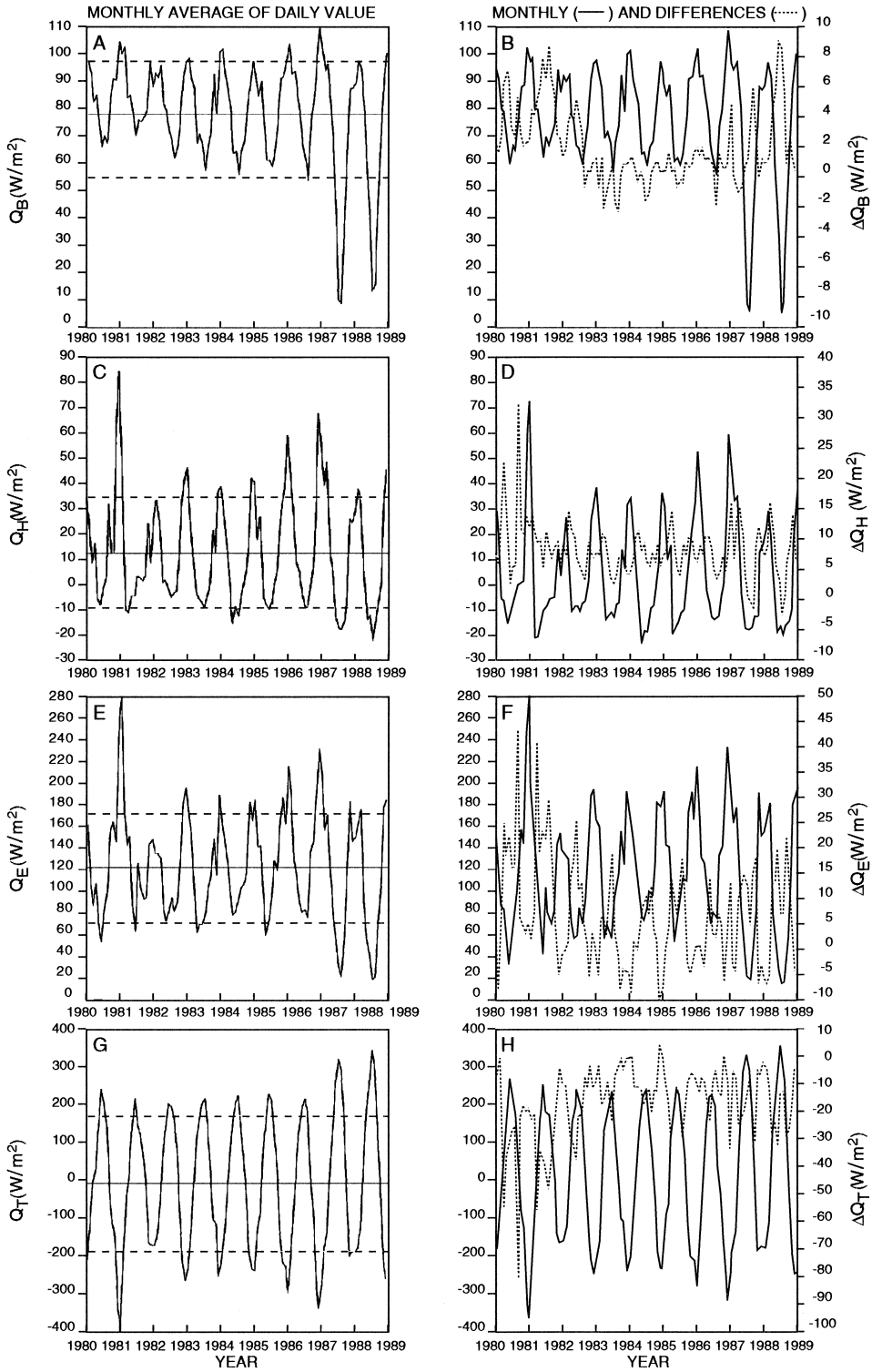


Fig. 4. Time series of surface monthly averaged Q_S for the period January 1980–December 1988. The interannual mean and ± 1 standard deviation lines are also indicated.



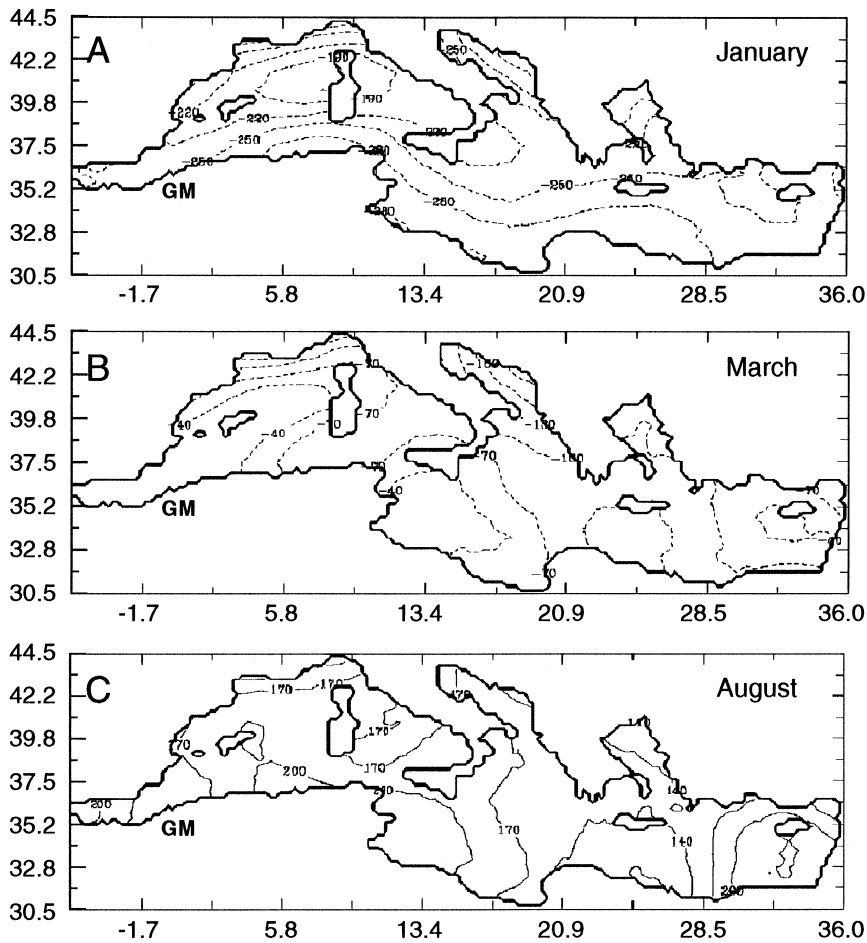


Fig. 6. Climatologies of Q_T ($CI = 30 \text{ W/m}^2$) for January (A), March (B) and August (C).

and 1988. Q_E and Q_H show the largest differences before and after the strong event of January 1981 (Fig. 5D, F). During winters, the MDS data can produce larger latent heat fluxes than those from DDS, while Q_H with DDS is always larger than with MDS.

The Q_T term shows large differences between DDS and MDS during the winters of 1980 and 1986, with the maximum difference at the end of 1980 (Fig. 5H). It is thus clear that the DDS data are

important to correct the budget during anomalous forcing events as in the case of the 1981 and 1986 winters.

In Fig. 6 we show the patterns of the climatological values of Q_T for 3 months (January (A), March (B) and August (C)). In January the north–south gradient of the Q_T field resembles the wind pattern, and there are maximum heat losses ($\sim 280 \text{ W/m}^2$) all along the southern coasts of the basin. In March (Fig. 6B) the situation has changed and the heat loss

Fig. 5. Left panels: time series of the surface monthly averaged heat fluxes calculated from DDS (exp. 6): Q_B (A), Q_H (C), Q_E (E) and Q_T (G). The interannual mean and ± 1 standard deviation lines are also indicated. Right panels: time series of the surface averaged monthly heat fluxes calculated from MDS (solid line) (exp. 3) and difference values between the DDS and MDS calculated fluxes (dashed line): Q_B and ΔQ_B (B), Q_H and ΔQ_H (D), Q_E and ΔQ_E (F), Q_T and ΔQ_T (H).

areas are now more concentrated in subbasin centers, one in the Western and three others in the Eastern Mediterranean. The summer conditions (August) are similar in pattern to March, but with positive values. The maximum heat gain of the sea surface (220 W/m^2) is in the south-eastern Levantine basin near Cyprus, while heat gain minima are located in the Balearic–Ligurian subbasin and on the eastern sides of the Adriatic and Aegean subbasins, the latter being a known area of summer upwelling. Over the Algerian basin Q_T has a strong seasonal variability from maximum heat loss in winter to maximum heat gain in summer.

It is important to emphasize that the climatological January Q_T shown in Fig. 6A for the known Mediterranean convection areas (Gulf of Lions, Adriatic basin, Levantine basin) range from -220 to -260 W/m^2 , which is too low if compared to the observed Q_T of -800 W/m^2 found by Leaman and Schott (1991) in the Gulf of Lions. This clearly shows that it is difficult to force realistic Mediterranean deep convection in OGCMs using climatological surface fluxes (Roussenov et al., 1995). We now examine the horizontal structure of the 1981, 1986, 1987 and 1988 anomalies.

4.2.1. Winter anomalies

In January and March 1981 we see minimum values of relative humidity reaching an average of 45% during March (Fig. 7A, B). The wind field has its largest anomaly in January 1981, when it appears that the Mistral regime can be detected over the whole basin (Fig. 7E, F). This anomalous wind field, especially over the Ionian basin, along with the air temperature anomaly is responsible for the highest values of Q_E (Fig. 7C, D) and Q_H (not shown here) of the whole time series. In January 1981 the Q_T field (Fig. 7G) shows the largest negative value of all the time series (surface average $Q_T = -387 \text{ W/m}^2$), in particular along the southern boundaries of the Ionian basin (Fig. 7G), where it has been shown that downwelling occurs by Roussenov et al. (1995).

In the winters of 1986 and 1987 (Fig. 8) we still find anomalous wind speeds and large minima of T_A and T_S . The Q_T field (Fig. 8E, F, G, H) is again dominated by Q_E , which shows in January 1986 an anomalous pattern compared to climatology, with large positive values south of Crete (Fig. 8A). The

fields of March 1986 (Fig. 8B, F) indicate that the transition to summer conditions is slightly faster than average since there are already some positive Q_T areas in both Western and Eastern subbasins (compared to climatological mean conditions of Fig. 6). It is interesting to note that the Q_T pattern of March 1986 is the least affected by Q_E , with large differences in the Ionian subbasin (Fig. 8F). In 1987 (Fig. 8G, H) we see increasing gradients of the fields over the whole basin, while the winter conditions last longer in the Western Mediterranean (Q_T still shows very negative values in March 1987). This suggests that the data obtained in winter 1987 in the Gulf of Lions (Leaman and Schott, 1991) were characteristic of a severe winter with numerous Mistral. The winter patterns of Q_E and Q_T for 1987 (Fig. 8B, D, G, H) show an horizontal pattern with multiple centers, very different from the smooth patterns of other 1986 winters (Fig. 8A, B, E, F).

In conclusion, the anomalous winters of 1981, 1986 and 1987 are all connected to anomalous wind stresses over the basin. In the case of 1981 the anomaly has a basin scale and is large in the Ionian and southern part of the Eastern Mediterranean basins. In 1986 and 1987 the anomalies are more local. In 1986 the largest anomaly in heat loss is again in the southern part of the Eastern Mediterranean basin while in 1987 it is in the Balearic–Ligurian area and Eastern Levantine basin.

4.2.2. Summer anomalies

We examine here the two anomalous August months of 1987 and 1988 compared to the August of 1986 (Fig. 9). Compared to an average summer, the major change in atmospheric parameters during the summer anomalies of 1987–1988 occurs in T_A (Fig. 9A, C, E). In general summer values of T_A increase in the whole basin, reaching an average of 34°C in August 1987. Furthermore there are increasing T_A gradients especially along the southern coastlines. The T_A anomaly is responsible for the anomaly in Q_E , which shows negative areas located in the Levantine basin (Fig. 9B, D, F). These areas of negative Q_E values represent the largest heat gain in the basin, and are due when the q_A term is larger than q_S term in the latent heat flux bulk formulation. This could imply processes of surface fog (condensation of water vapor over the sea surface) which are

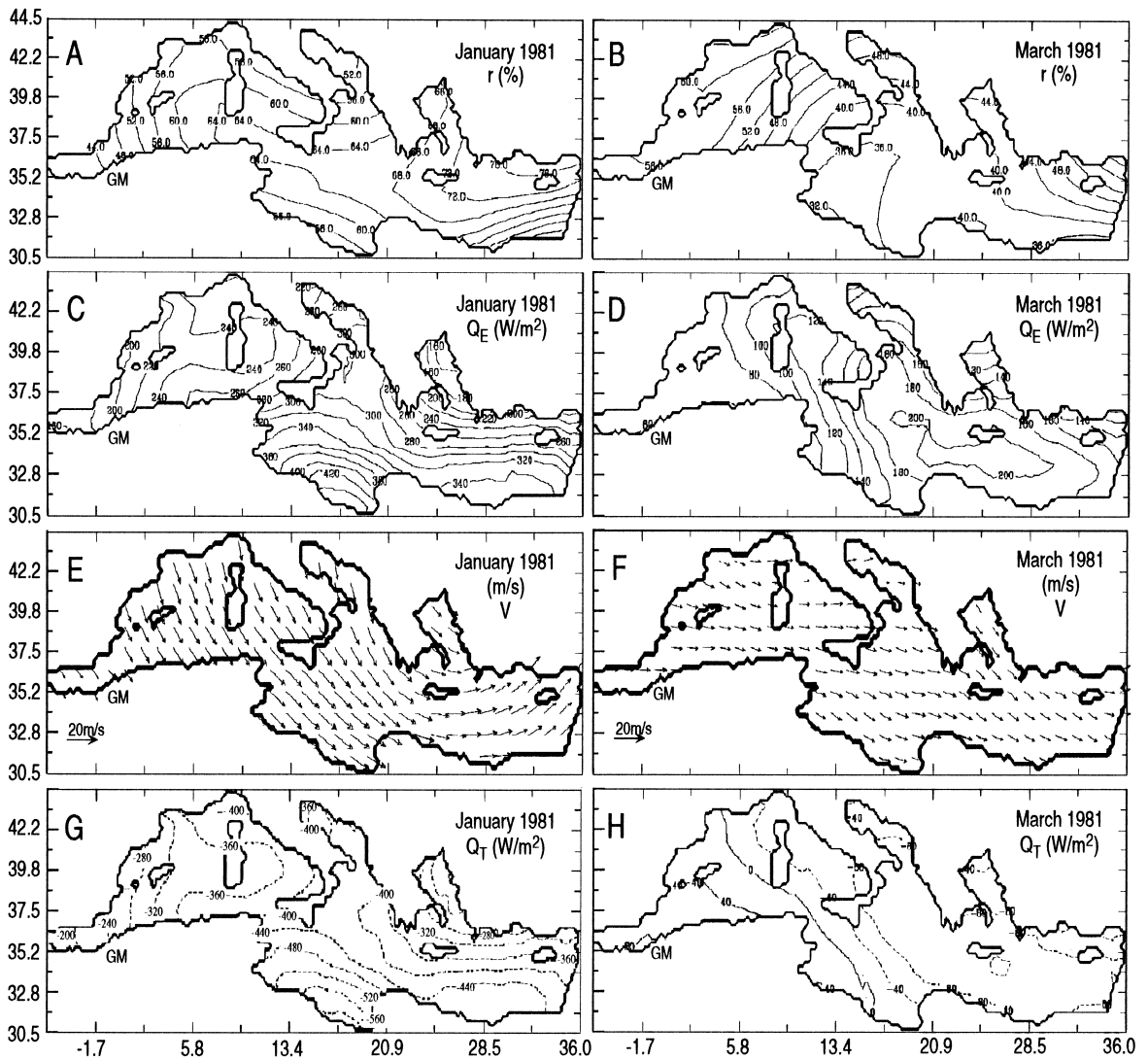


Fig. 7. Monthly averaged r , Q_E , $|\vec{V}|$ and Q_T fields for 1981 (exp. 6): r (CI = 4%) for January (A) and March 1981 (B), Q_E (CI = 20 W/m^2) for January (C) and March 1981 (D), $|\vec{V}|$ for January (E) and March 1981 (F), Q_T (CI = 40 W/m^2) for January (G) and March 1981 (H).

difficult to be parameterized by traditional bulk formulations. These large q_A values are produced by high air temperatures in these summer months of the NMC data set. These anomalous areas also affect the average value of Q_E for the whole basin, which goes from 78 W/m^2 for August 1986 to 22 W/m^2 for August 1987. The 1987 and 1988 summer anomalies are also well pronounced in the rest of the Mediterranean basin corresponding to a more than 50%

decrease of the average Q_E . In contrast, the wind pattern (not shown) during these summers does not show any anomalous behaviour with respect to its climatology.

4.3. Error analysis

Several factors, related to random and systematic errors, can affect the validity of Mediterranean heat

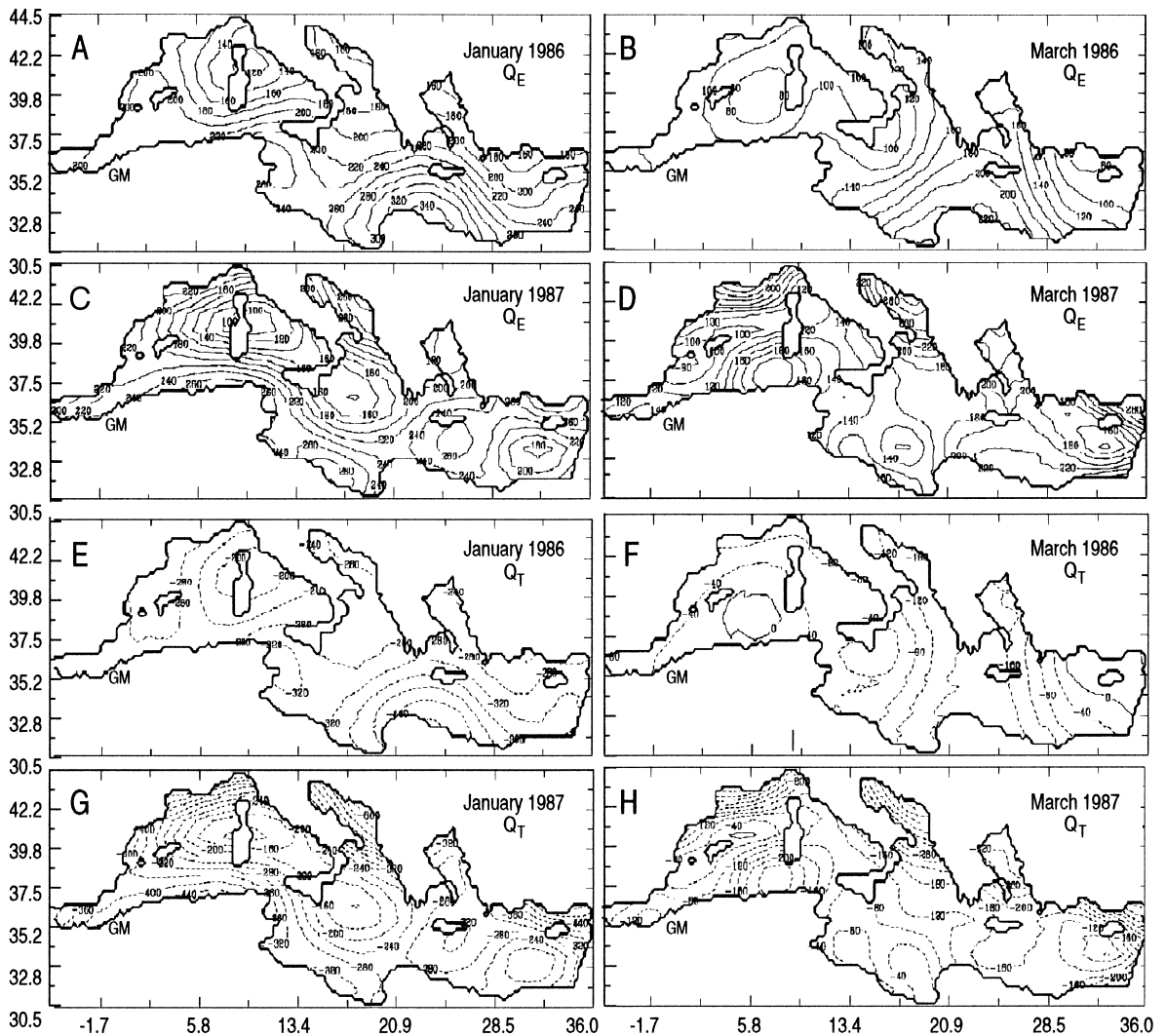


Fig. 8. Monthly averaged Q_E and Q_T fields for 1986–1987 (exp. 6): Q_E (CI = 20 W/m^2) for January (A) and March 1986 (B), Q_E (CI = 20 W/m^2) for January (C) and March 1987 (D), Q_T (CI = 40 W/m^2) for January (E) and March 1986 (F), Q_T (CI = 40 W/m^2) for January (G) and March 1987 (H).

budget estimates. The NMC data, being a model generated data set, have the significant advantage of a complete coverage in time and space (although with some missing or bad data), which reduces the problem of inadequate sampling. Nevertheless, this data set has systematic errors which can be hard to estimate. A few studies (Trenberth et al., 1987; Trenberth and Olson, 1988a,b) have estimated the impacts of different operational changes on the NMC

analyses, but only the reanalysis of the original data would determine the validity of NMC analyses for climate investigations. As an extreme case, we could consider the NMC analysis errors to be of the same magnitude as the assimilated data errors in the NMC spectral model (1°C for T_A , 3 m/s for wind and 10% for relative humidity). For the other data sets (Reynolds and COADS) we assume global error estimates values of 0.78°C for T_S and 0.2 for cloud

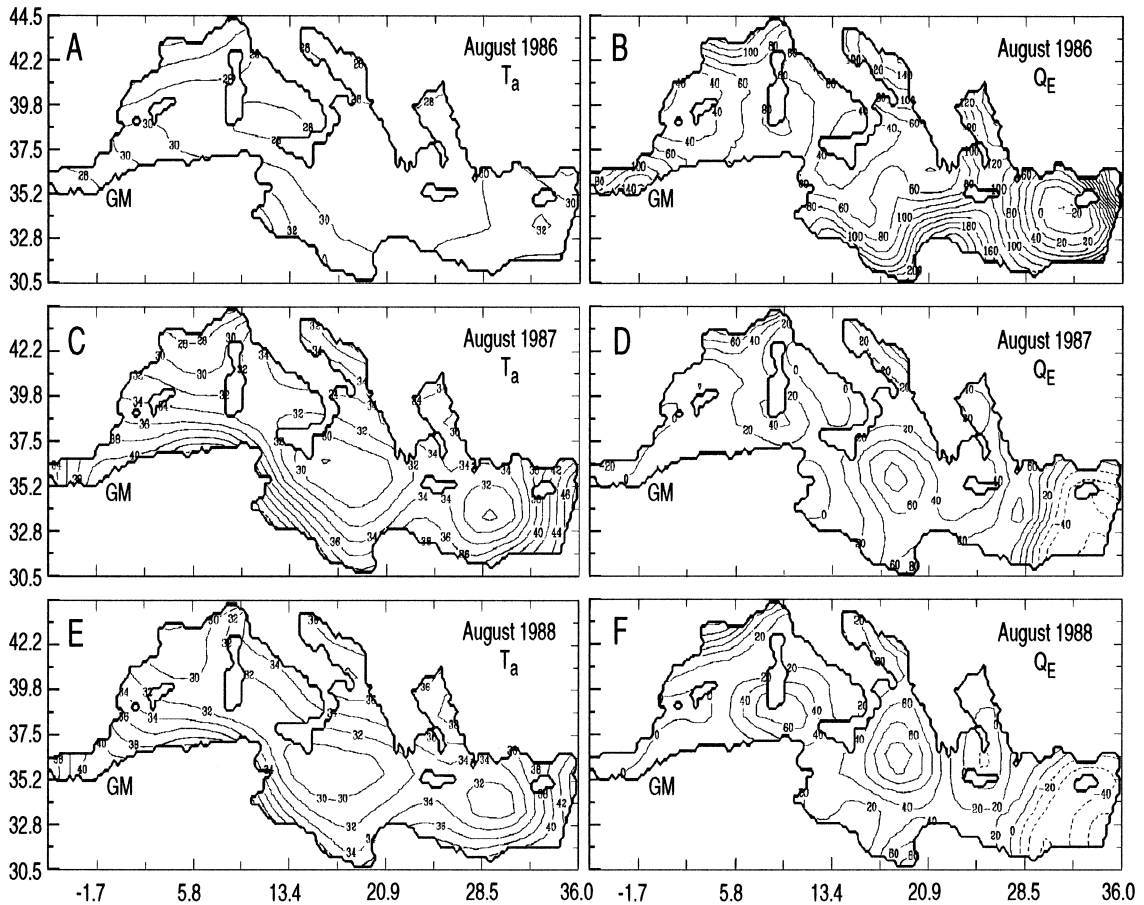


Fig. 9. Monthly averaged T_A and Q_E (exp. 6) for August 1986–1988: T_A (CI = 2°C) for August 1986 (A), August 1987 (C) and August 1988 (E), Q_E (CI = 20 W/m²) for August 1986 (B), August 1987 (D) and August 1988 (F).

cover (Reynolds, 1988; Gilman and Garrett, 1994). Instead the uncertainty of the albedo estimations, following Payne (1972) method, is about 7%.

Systematic errors can arise from using the bulk formulas with inappropriate data, for example using data not at the standard 10 m level. Using the 1000 hPa NMC data with a variable elevation (not always 10 m) would introduce a bias in our estimates; however, quantifying this would be quite difficult. Random errors can also affect the formulations discussed above. Simpson and Paulson (1979) and Dobson and Smith (1988) found that the *Reed* empirical formula for solar radiation was the best available compared to observations but was still affected by large random errors. The formulas for net outgoing longwave radiation flux present the same problems; large uncertainties in cloud cover, temperature and

humidity, together with a lack of verification at the ocean surface (since they have been derived mostly on land). Fung et al. (1984) found the mean values estimated by different formulas to have uncertainties of around ± 15 W/m², while Simpson and Paulson (1979) found random errors of about ± 5 W/m². Schiano et al. (1993), by comparing their experimental results with those of some bulk formulas for Q_B , found a bias of -30 W/m² and a rms error larger than ± 30 W/m². In particular the *Brunt* and *Berliand–Berliand* formulas gave the smallest bias and rms errors. Therefore, following their results, our computed values would have an estimated uncertainty of $\sim 40\%$.

Blanc (1985, 1987), comparing 10 different schemes for computing sensible and latent heat fluxes, estimated the random error to be around

$\pm 25\%$. A minimum desired accuracy for heat budget estimates would be $\pm 10 \text{ W/m}^2$ (Fung et al., 1984).

In this study we have estimated, as simply as possible, the random errors of the heat budget components calculated only with the DDS data, since we consider them our best results. We calculate the standard deviations of each parameter of the 12-hourly NMC data, removing the seasonal signal, and we assume these to be a reasonable estimate of the random errors of each parameter. We average them on the Mediterranean basin and, assuming all errors to be random, the uncertainties in the sample mean heat budget would reduce by $1/\sqrt{N}$, where N is the number of independent observations. If the nonannual-cycle signals are uncorrelated between years, N should be 9. However, since this signal appears to be only weakly correlated between the Eastern and Western basins, we choose $N = 18$ degrees of freedom.

In the case of the cloud cover and T_s data we use the estimate of their global errors described above. We then apply an error propagation scheme to the fluxes Q_s , Q_b , Q_h and Q_e , assuming a linear dependence of their errors on the meteorological parameters, and we estimate the uncertainties to be $R_{Q_s} = \pm 5 \text{ W/m}^2$, $R_{Q_b} = \pm 7 \text{ W/m}^2$, $R_{Q_h} = \pm 4 \text{ W/m}^2$ and $R_{Q_e} = \pm 8 \text{ W/m}^2$, respectively.

Hence, the total uncertainty R_{Q_T} of the derived Q_T values is calculated by:

$$R_{Q_T} = \pm \sqrt{(R_{Q_s})^2 + (R_{Q_b})^2 + (R_{Q_h})^2 + (R_{Q_e})^2} \\ \sim \pm 12 \text{ W/m}^2 \quad (6)$$

This suggests that only the DDS experiments (4–7 in Table 6) provide Q_T values which are negative as needed to satisfy the Mediterranean closure problem.

5. Sensitivity of OGCM to air–sea interaction physics

The Mediterranean heat budget closure problem has allowed us to define a set of calibrated air–sea physics parameterizations which are consistent with the Gibraltar heat flux constraint. This calibrated set of bulk formulas are now used to force an OGCM

implemented in the Mediterranean area (Roussenov et al., 1995; Pinardi et al., 1997). We would like now to show the importance of using the calibrated air–sea physics in order to correctly simulate the surface and intermediate temperature structure.

The NMC and the COADS cloud coverage data set have been averaged to create climatological values of wind, air temperature, relative humidity and clouds (a year of monthly means). We call this ‘perpetual year data’ since we will use it repeatedly every year of integration of the model. The atmosphere then repeats its climatological values, but the T_s values are coming from the model itself, and all these data are used to estimate the momentum and heat fluxes to force the model. We refer to this scheme as an ‘interactive air–sea interaction scheme’ (IASIS).

The model used is the MOM-GFDL as developed by Pacanowski et al. (1991) on the previous work of Cox (1984). It is a three dimensional primitive equation model implemented for this study in the Mediterranean basin with 0.25×0.25 degrees of horizontal resolution, 19 levels and it is described in details in Roussenov et al. (1995). The Strait of Gibraltar is open adjacent to an Atlantic box where the inflow is modelled by a Newtonian relaxation to climatological temperature and salinity at all levels. This open boundary condition (‘sponge layer’) has been used in the past by Philander et al. (1987), Bryan and Holland (1989) to represent poorly resolved areas of OGCMs, and later in the Mediterranean by Roussenov et al. (1995), Castellari (1996) and Pinardi et al. (1997). Instead of the surface water fluxes dependent on the evaporation–precipitation (E–P), the Newtonian relaxation to a monthly mean salinity has been used because of the unreliability of precipitation data over marine areas. Then the ‘implied E–P’ flux in the model is:

$$W_F = \frac{dz(S^* - S)}{\tau S} \quad (7)$$

where dz is the first layer thickness, S^* is the climatological sea surface salinity field, S is the model sea surface salinity and τ is the damping time scale.

We carried out three numerical experiments only differing by the set of bulk formulations needed to

estimate the heat fluxes at the model surface. We called PA1 the experiment with the same set of bulk formulations of Test 1 of Table 6; PA2 the experiment with the same set of bulk formulations of Tests 2 and 4 of Table 6; and finally PA3 the experiment with the same set of bulk formulations of Tests 3 and 6 of Table 6. Then the PA3 experiment uses as a top boundary condition for the temperature the calibrated set of heat flux formulations.

The model results have been analyzed after 10 years of model integrations. We estimated the heat budget (Q_{TM}) and the net advective heat flux (G_{HM}) averaged over the Mediterranean Basin from the model results. Also we computed the net heat residual (R_{HM}) as the difference between Q_{TM} and G_{HM} , which on a long term average should be zero (Table 7).

The calibrated set of formulations (PA3) produces the smallest Q_{TM} value. The calibration hierarchy of the three sets of formulations is strongly confirmed by the model response, giving ourselves more confidence in the calibration results of the previous sections. We consider the resulting values of Q_{TM} for PA3 reasonable considering the climatological forcing used.

All our model versions give positive values (Table 7), showing that there is a warm bias in the modelled Mediterranean temperatures. We refer to this as a ‘model systematic error’. Despite this problem, the PA3 run produce the minimum heat residual (3.7 W/m^2) which can be considered a promising

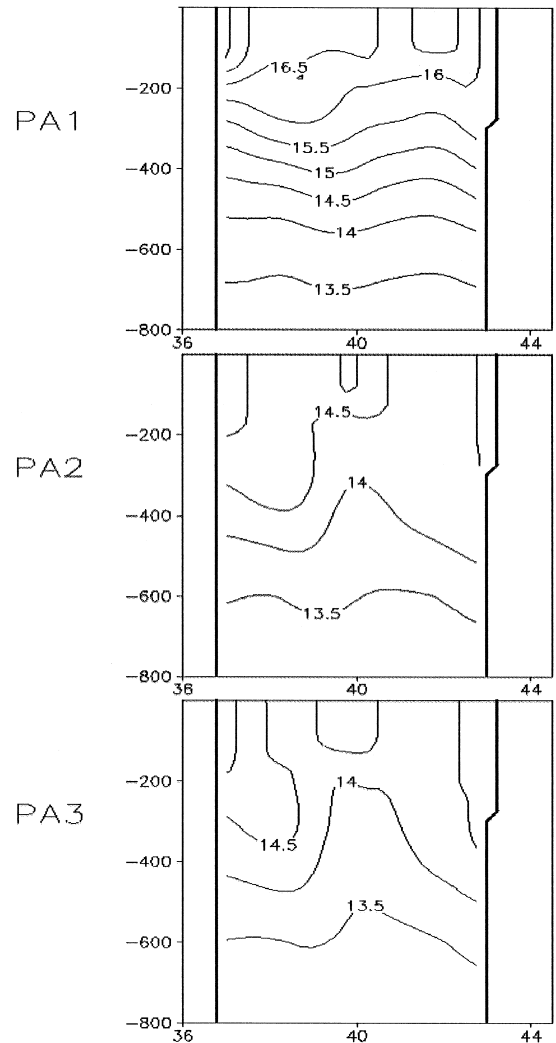


Fig. 10. Gulf of Lions section of temperature with different air–sea interaction physics for the month of February. The name of the experiment is given on the left of each picture. Experiments are described in Table 7. The section is at 4.75°E and extends latitudinally across the basin as shown by Fig. 1.

Table 7

Three OGCM experiments done with different sets of heat fluxes bulk formulations as temperature surface boundary conditions

Exp.	Q_{TM}	G_{HM}	R_{HM}
PA1	6.2	2.2	8.4
PA2	1	3.3	4.3
PA3	0.3	3.4	3.7

PA1 uses the set of bulk formulations of Test 1 of Table 6.

PA2 uses the set of bulk formulations of Tests 2 and 4 of Table 6.

PA3 uses the set of bulk formulations of Tests 3 and 6 of Table 6.

Q_{TM} (in W/m^2) is the surface heat budget estimated by the OGCM.

G_{HM} (in W/m^2) is the heat transport at the Strait of Gibraltar averaged over the Mediterranean area.

$R_{HM} = Q_{TM} - G_{HM}$ is the net residual.

If the OGCM is heat balanced the R_{HM} should be close to 0.

result. The model parameterized water fluxes averaged over the Mediterranean Basin in a year are 0.30 m/yr for PA1 and 0.22 m/yr for PA2 and PA3. These values are lower than the observational values from Table 4 or from the value (0.66 m/yr) estimated from the work of Peixoto et al. (1982), but the latent heat fluxes Q_E are correctly taken in account. In fact the averaged Q_E from the model experiments

range from 112 W/m^2 to 122 W/m^2 which is consistent with the water budget range of Table 4 and the past results of Table 1.

It is possible now to analyze the vertical temperature structures simulated by the model as a function of the three different physics. We present sections

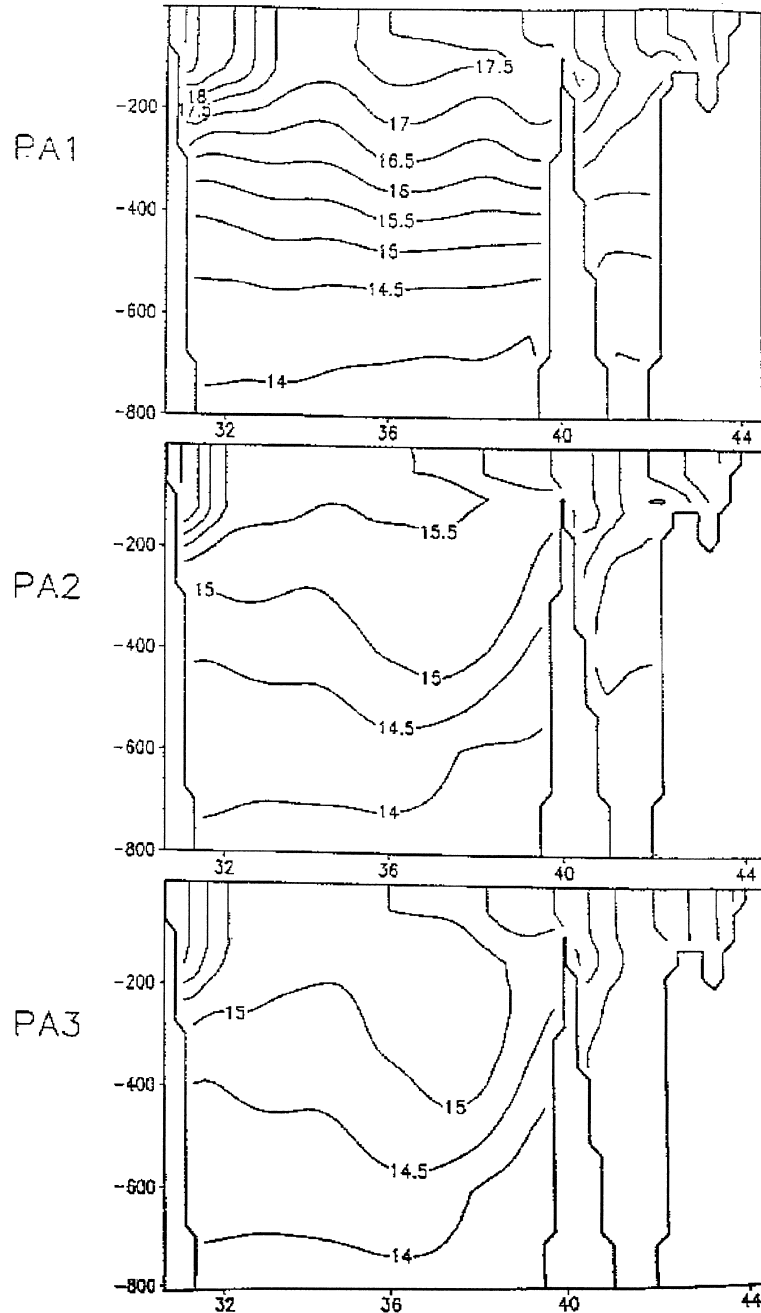


Fig. 11. Adriatic-Ionian section of temperature with different air-sea interaction physics for the month of February. The name of the experiment is given on the left of each picture. Experiments are described in Table 7. The section extends across the Adriatic Basin and latitudinally at 18.05°E across the Ionian Basin as shown by Fig. 1.

across the Gulf of Lions (Fig. 10), the Adriatic-Ionian area (Fig. 11) and the Rhodes area (Fig. 12) for the month of February of the 10th year of integration. The difference between PA1, PA2, PA3 is striking in all the three figures.

In Fig. 10 the PA1 water column is too warm (16.5°C at the surface) and the thermocline has shifted vertically down to 500 m, while the PA2 water column is less stratified and the temperatures

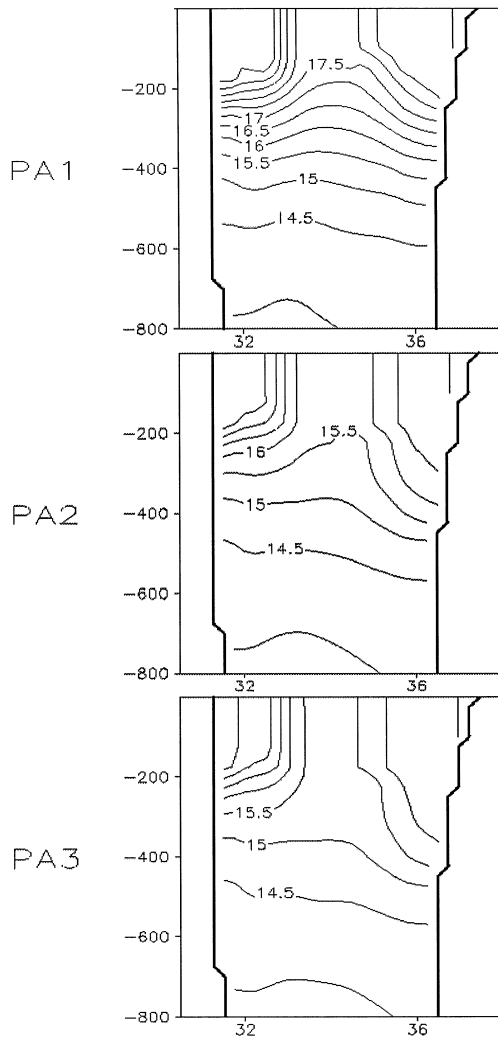


Fig. 12. Rhodes section of temperature with different air–sea interaction physics for the month of February. The name of the experiment is given on the left of each picture. Experiments are described in Table 7. The section is at 27°E and extends latitudinally across the Levantine Basin as shown by Fig. 1.

have decreased ($15\text{--}14^{\circ}\text{C}$ at the surface) to known surface values, but only the PA3 (model version with our calibrated formulation) water column is well unstratified in February, the values of temperatures are reasonable and the cyclonic Lions Gyre is well formed (the dome is developed with its top at 200 m). However, even the PA3 run does not give correct deep water formation in the Lions Gulf, since the mixed layer water has properties ($T = 14^{\circ}\text{C}$, $S = 38$ psu and thus a density of $\sigma_T = 28.5$) lighter than a typical deep water in that region which should have a climatological surface density of $\sigma_T = 28.9$ (Madec et al., 1991).

In the Adriatic area (Fig. 11) the PA1 and PA2 runs have produced unrealistic high temperatures (a $14\text{--}16^{\circ}\text{C}$ range for PA1 and a $12.25\text{--}14.5^{\circ}\text{C}$ range for PA2 at 800 m depth), while the PA3 shows a quite realistic range of $11.25\text{--}13^{\circ}\text{C}$. The water formation is still not correct, because this water is too light ($\sigma_T = 28.9$ in the southern Adriatic area) compared with observations (Ovchinnikov et al., 1987; Artegiani et al., 1997), due mainly to low salinity values ($S \sim 38.3$ psu).

In the Rhodes area (Fig. 12) the PA1 run gives again large temperatures ($T > 17^{\circ}\text{C}$) producing a LIW water too light ($\sigma_T \sim 28.4$), which does not convect to the base of the thermocline, while the PA2 temperatures are lower, but only the PA3 run produces sufficiently low temperatures ($T = 15.25^{\circ}\text{C}$) to form a LIW water ($\sigma_T = 28.9$) which is at the lowest limit values found in the observations (Lascaratos et al., 1993). However, in general, we notice that also with the calibrated air–sea interaction physics the thermocline is too deep, due to the large vertical mixing ($1\text{ cm}^2/\text{s}$) and the relatively coarse vertical resolution of our model.

To evaluate more quantitatively the effect of the calibrated air–sea physics on the seasonal cycle, we have taken, for the different model runs, the difference between monthly mean model SST and the climatological SST extracted from the work of Reynolds (1982). In Fig. 13 we show the difference fields for February and July. The PA3 winter fields show a marked improvement with an average error reduction of 2°C . However, the improvement is lower during the summer ($\sim 1^{\circ}\text{C}$) and generally still large $2\text{--}4^{\circ}\text{C}$ errors are present along the boundary areas. The model systematic error can be then connected to

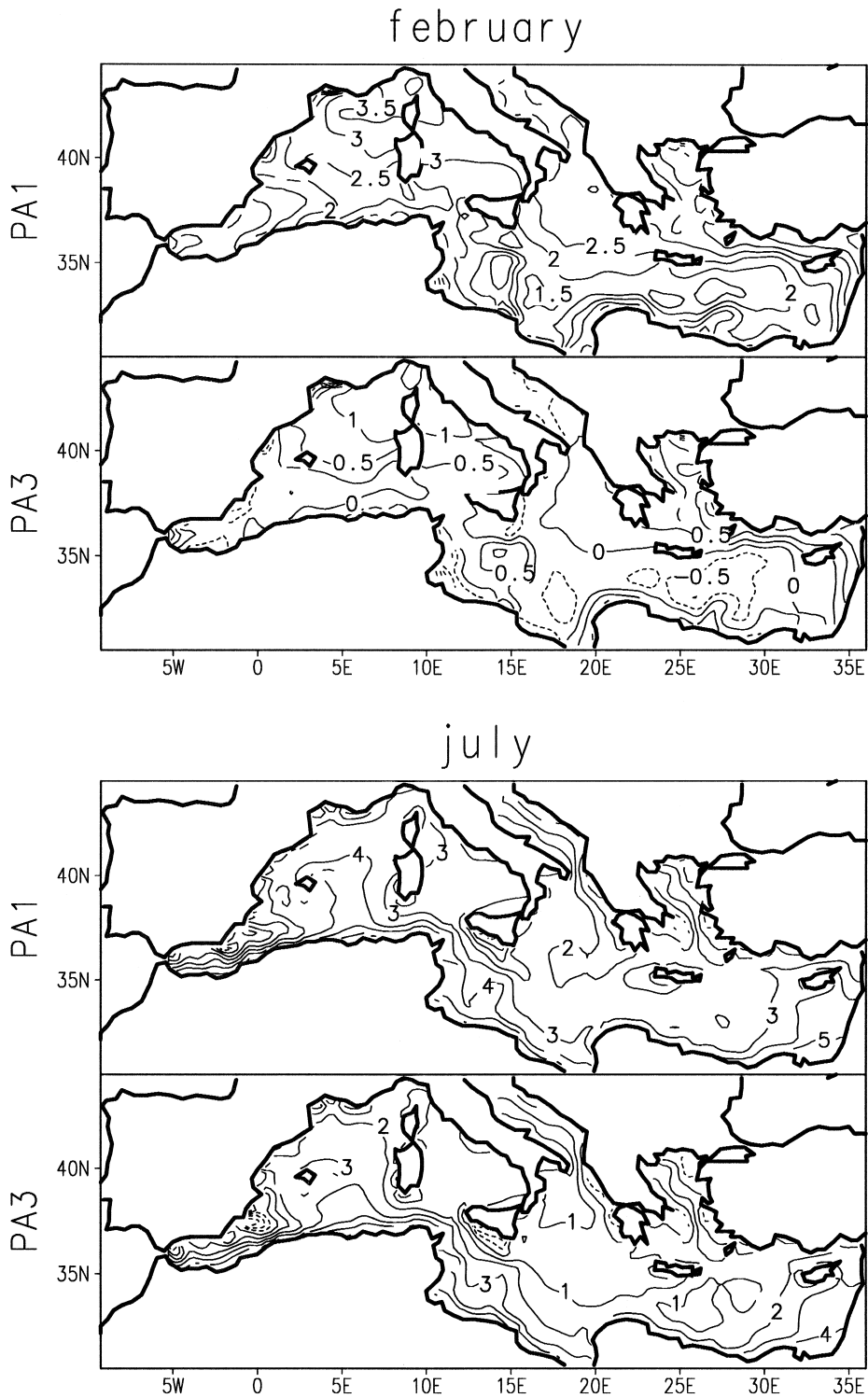


Fig. 13. February (CI = 0.5°C) and July (CI = 1°C) maps of sea surface temperature (SST) differences between Reynolds monthly mean climatology and model results for two different model versions: PA1 and PA3.

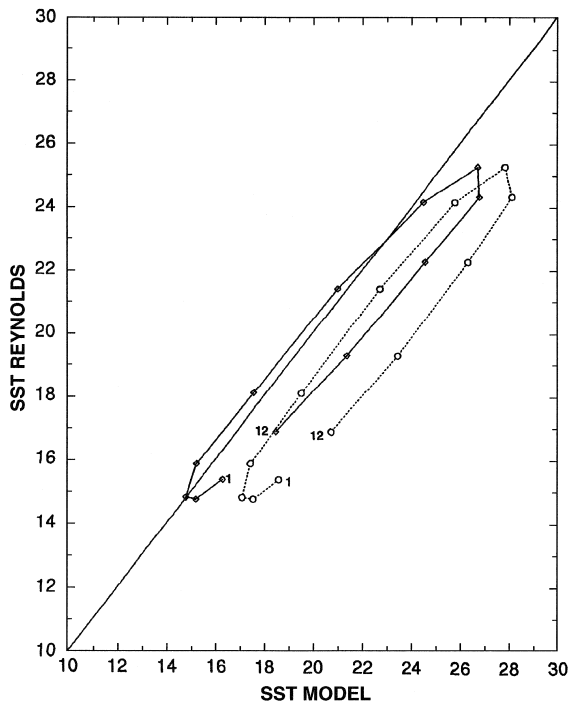


Fig. 14. Correlation plot of 12 monthly mean model SST with climatological Reynolds SST for PA1 and PA3 runs. PA1: ○ and dashed line PA3: □ and solid line (The numbers 1 and 12 correspond to the January and December values).

summer months higher temperatures or to a warm bias in the modelled temperatures as said before.

In order to quantify this bias we have taken the correlation between basin averaged modelled and Reynolds SST. The correlation is shown in Fig. 14 for the PA1 and the basin PA3 cases. The improvement introduced by the PA3 experiment is again marked but the warm bias is still present.

In summary, these experiments show that the use of calibrated air–sea interaction physics has a beneficial impact on model performance to reproduce SST values and water column structures. We have also shown that the amount of model systematic error can be partially controlled by the choice of air–sea physics for the model.

6. Conclusions

In the first part of the paper, we have analyzed different bulk formulations representing the heat

budget components of the Mediterranean Sea. We have used twice daily 1000 hPa analyses from NMC with COADS cloud cover and Reynolds T_S for the period 1980–1988.

The Mediterranean puts a formidable constraint on the correct long term mean basin averaged Q_T since there is a net heat inflow at Gibraltar ($7 \pm 3 \text{ W/m}^2$). Furthermore, the terrestrial branch of the Mediterranean water cycle gives a range of values for E (1.32–1.57 m/yr) limiting in turn the range of the latent heat flux. We call this the heat budget closure problem of the Mediterranean Sea.

Firstly, we have shown that it is possible to calibrate a set of air–sea physics parameterizations with atmospheric operational analyses in order to obtain a negative Mediterranean Sea heat budget. We call these formulations the ‘calibrated set’ of air–sea physics parameterizations for the Mediterranean Sea.

Using DDS data with the *May* formula for Q_B and the *Kondo* scheme for Q_H and Q_E we obtained a long-term mean value of $Q_T = -11 \text{ W/m}^2$, which is in close agreement with the observations. The negative value of Q_T is produced by a large increase of Q_H in the balance (Table 6). In this case, the equivalent evaporation is 1.57 m/yr, which is still within the expected range. Our results clearly show that the high frequency signal in the meteorological parameters improves the climatological heat budget estimate.

The outstanding interannual signals in all components of Q_T are due to anomalies in the atmospheric parameters, which are driven by sporadic events occurring separately in the Western and Eastern Mediterranean basins (such as for T_A in the summers of 1987 and 1988) or by basin wide events (such as the Mistral in January 1981). The winter heat budget anomalies are mainly associated with large wind anomalies whereas the summer ones are associated with air temperature anomalies especially over the Eastern Mediterranean.

Different sets of air–sea interaction bulk formulas have been used to force an OGCM of the whole Mediterranean. Three different sets of air–sea formulations have been tried and intercompared. Each model was integrated for 10 years and then the results displayed. We have shown that the calibrated set of air–sea interaction bulk formulas can markedly improve the water mass representation of the OGCM,

in particular producing a realistic LIW formation in the Levantine basin. The calibrated set improves the ability of the OGCM to generate realistic subsurface oceanic features such as the cyclonic gyre in the Gulf of Lions and helps to reduce the systematic error of the model decreasing the warm climate bias.

This work stresses the importance of having an appropriate temperature air–sea boundary condition for OGCM applied to special areas such as the Mediterranean Sea. Future work will involve carrying out experiments with the calibrated temperature air–sea boundary condition along with high frequency forcing data such as NMC (12-hourly) or ECMWF (6-hourly).

Acknowledgements

We would like to thank Mr. A. Rosati (GFDL-NOAA, Princeton, NJ, USA) and Dr. A. Oort (GFDL-NOAA, Princeton, NJ, USA), who have given us the NMC data and the COADS data. We appreciate also the assistance provided by Dr. G. Korres (Athens University, Greece), Dr. A. Navarra (IMGA-CNR, Bologna, Italy), Mrs. Jean Carpenter (RSMAS, University of Miami, FL, USA) and Ms. Elisabetta Masetti (IMGA-CNR, Bologna, Italy). This work was partially supported by NSF grant OCE-91 15995 and by the MAST contract 0039-(C), ‘MERMAIDS’ and MAS2-CT93-0055, ‘MERMAIDS-II’.

References

- Artegiani, A., Bregant, D., Paschini, E., Pinardi, N., Raicich, F., Russo, A., 1997. The Adriatic general circulation. Part I: Air–sea interactions and water mass structure. *J. Phys. Oceanogr.* 27, 1492–1514.
- Berliand, M.E., Berliand, T.G., 1952. Determining the net longwave radiation of the earth with consideration of the effect of cloudiness. *Isv. Akad. Nauk. SSSR Ser. Geofis.* 1.
- Bethoux, J.P., 1979. Budgets of the Mediterranean Sea: their dependence on the local climate and on the characteristics of the Atlantic waters. *Ocean. Acta* 2, 157–163.
- Bethoux, J.P., Gentili, B., 1994. The Mediterranean Sea, a test area for marine and climatic interactions. In: Malanotte-Rizzoli, P., Robinson, A.R. (Eds.), *Ocean Processes in Climatic Dynamics: Global and Mediterranean Examples*. NATO ASI Series, Vol. 419, pp. 239–251.
- Bignami, F., Santoleri, R., Schiano, M., Marullo, S., 1991. Net longwave radiation in the Western Mediterranean Sea. Poster Session at the 20th General Assembly of the International Union of Geodesy and Geophysics, IAPSO, Vienna.
- Bignami, F., Marullo, S., Santoleri, R., Schiano, M.E., 1995. Longwave radiation budget in the Mediterranean Sea. *J. Geophys. Res.* 100 (C2), 2501–2514.
- Blanc, T.V., 1985. Variation of bulk-derived surface flux, stability and roughness results due to the use of different transfer coefficient schemes. *J. Phys. Oceanogr.* 15, 650–669.
- Blanc, T.V., 1987. Accuracy of bulk-method-determined flux, stability, and sea surface roughness. *J. Geophys. Res.* 92, 3867–3876.
- Boyum, G., 1967. Hydrology and currents in the area West of Gibraltar. Tech. Rep. 36 and NATO sub-Committee on Oceanographic Research.
- Bryan, F.O., Holland, W.R., 1989. A high resolution simulation of the wind and thermohaline driven circulation in the North Atlantic Ocean. In: Muller, P., Henderson, D. (Eds.), *Parametrizations of Small-Scale Processes*, Proceedings of the Hawaiian Winter Workshop, special publication. Hawaii Inst. of Geophys., University of Hawaii at Manoa.
- Bryden, H.L., Kinder, T.H., 1991a. Steady two-layer exchange through the Strait of Gibraltar. *Deep-Sea Res.* 38, 445–463, Suppl. 1.
- Bryden, H.L., Kinder, T.H., 1991b. Recent progress in strait dynamics. *Rev. Geophys., Supplement*, pp. 617–631.
- Budyko, M.I., 1963. Atlas of the heat balance of the earth. *Glabnaia Geofiz. Observ.*
- Budyko, M.I., 1974. *Climate and Life*. Academic Press, New York, 508 pp.
- Bunker, A.F., Charnock, H., Goldsmith, R.A., 1982. A note on the heat balance of the Mediterranean and Red Seas. *J. Mar. Res.* 40, 73–84, Suppl.
- Castellari, S., 1996. A numerical study of water mass formation processes and seasonal to interannual variability in the Mediterranean Sea. PhD dissertation, RSMAS, University of Miami, FL, USA.
- Castellari, S., Pinardi, N., 1992. A realistic General Circulation Model of the Mediterranean Sea: II. Final analysis of surface meteorological data. IMGA-CNR Tech. Rep. No. 1–92, Modena, Italy. Available from IMGA, Via Gobetti 101, Bologna, Italy.
- Castellari, S., Pinardi, N., Navarra, A., 1990. A realistic General Circulation Model of the Mediterranean Sea: I. Surface energy parameterizations and meteorological forcing data sets. IMGA-CNR Tech. Rep. No. 4-90, Modena, Italy. Available from IMGA, Via Gobetti 101, Bologna, Italy.
- Cox, M.D., 1984. A primitive equation, 3-dimensional model of the ocean. GFDL Ocean Group Tech. Rep. No. 1, 143 pp.
- Dobson, J.W., Smith, S.D., 1988. Bulk models of solar radiation at sea. *Q. J. R. Meteorol. Soc.* 114, 165–182.
- Fung, I.Y., Harrison, D.E., Lacis, A.A., 1984. On the variability of the net longwave radiation at the ocean surface. *Rev. Geophys. Space Phys.* 22 (2), 177–193.
- Garrett, C., Outerbridge, R., Thompson, K., 1993. Interannual variability in Mediterranean heat and buoyancy fluxes. *J. Climate* 6, 900–910.

- Gill, A.E., 1982. *Atmosphere–Ocean Dynamics*. Academic Press, New York, 662 pp.
- Gilman, C., Garrett, C., 1994. Heat flux parameterizations for the Mediterranean Sea: the role of atmospheric aerosols and constraints from the water budget. *J. Geophys. Res.* 99 (C3), 5119–5134.
- Gulev, S., 1994. Influence of space–time averaging on the ocean–atmosphere exchange estimates in the North Atlantic Midlatitudes. *J. Phys. Oceanogr.* 24, 1236–1255.
- Hanawa, K., Toba, Y., 1987. Critical examination of estimation methods of long-term mean air–sea heat and momentum transfers. *Ocean–Air Interactions* 1, 79–93.
- Heburn, G.W., 1994. The dynamics of the seasonal variability of the Western Mediterranean circulation. In: La Violette, P.E. (Ed.), *Seasonal and Interannual Variability of the Western Mediterranean Sea*, Vol. 46. Coastal Estuarine Stud., AGU, Washington, DC, pp. 249–285.
- Hellermann, S., Rosenstein, M., 1983. Normal wind stress over the world ocean with error estimates. *J. Phys. Oceanogr.* 13, 1093–1104.
- Hsiung, J., 1986. Mean surface energy fluxes over the global ocean. *J. Geophys. Res.* 91, 10585–10606.
- Isemer, H.J., Hasse, L., 1987. The Bunker climate atlas of the North Atlantic. *Air–Sea Interactions*, Vol. 2. Springer Verlag, 252 pp.
- Isemer, H.J., Willebrand, J., Hasse, L., 1989. Fine adjustment of air–sea energy flux parameterizations by direct estimates of ocean heat transport. *J. Climate* 2, 1173–1184.
- Jaeger, L., 1976. Monatskarten des Niederschlags für die ganze Erde. *Berichte des Deutschen Wetterdienstes* 18, 38.
- Jones, C.S., Legler, D., O'Brien, J.J., 1993. Variability of surface fluxes over the Indian Ocean; 1960–1989. *The Atmosphere–Ocean System*, in print.
- Kondo, J., 1975. Air–sea bulk transfer coefficients in diabatic conditions. *Boundary-Layer Meteorol.* 9, 91–112.
- Lacombe, H., Tchernia, P., Richez, C., Gamberoni, L., 1964. Deuxieme contribution a l'etude du regime du detroit de Gibraltar. *Cah. Oceanogr.* 16, 283–327.
- Laevastu, T., 1967. Cloud factor in long-wave radiation formulas. *J. Geophys. Res.* 72, 4277.
- Lascaratos, A., Williams, R.G., Tragou, E., 1993. A mixed-layer study of the formation of Levantine Intermediate Water. *J. Geophys. Res.* 98 (C8), 14739–14749.
- Leaman, K.D., Schott, F.A., 1991. Hydrographic structure of the convection regime in the Gulf of Lions: winter 1987. *J. Phys. Oceanogr.* 21, 575–598.
- Legates, D.R., Willmott, C.J., 1990. Mean seasonal and spatial variability in gauge-corrected, global precipitation. *Int. J. Climatol.* 10, 111–127.
- List, R., 1958. *Smithsonian Meteorological Tables*. Smithsonian Institution, Washington, DC, 527 pp.
- Lowe, P.R., 1977. An approximating polynomial for the computation of saturation vapor pressure. *J. Appl. Meteorol.* 16, 100–103.
- Lumb, F.E., 1964. The influence of cloud on hourly amount of total solar radiation at the sea surface. *Q. J. R. Meteorol. Soc.* 90, 43–56.
- Macdonald, A., Candela, J., Bryden, H.L., 1994. An estimate of the net heat transport through the Strait of Gibraltar, Vol. 46. *Coastal Estuarine Stud.*, AGU, Washington, DC.
- Madec, G., Chartier, M., Delecluse, P., Crepon, M., 1991. A three-dimensional numerical study of deep-water formation in the Northwestern Mediterranean Sea. *J. Phys. Oceanogr.* 21, 1349–1371.
- Malanotte-Rizzoli, P., Bergamasco, A., 1991. The wind and thermally driven circulation of the eastern Mediterranean Sea: II. The Baroclinic case. *Dyn. Atmos. Oceans* 15, 355–419.
- May, P.W., 1986. A brief explanation of Mediterranean heat and momentum flux calculations. *NORDA Code 322, NSTL, MS 39529*.
- Millot, C., 1991. Mesoscale and seasonal variabilities of the circulation in the Western Mediterranean. *Dyn. Atmos. Oceans* 15, 179–214.
- Oberhuber, J.M., 1988. An atlas based on the COADS data set: the budgets of heat, buoyancy and turbulent kinetic energy at the surface of the global ocean. *Max-Planck-Institut für Meteorologie, Report No. 15*.
- Oort, A.H., Pan, Y., 1985. Diagnosis of historical ENSO events. *Proceedings of First WMO Workshop on the Diagnosis and Prediction of Monthly and Seasonal Variations over the Globe*, College Park, MD.
- Ovchinnikov, I.M., Zats, V.I., Krivosheya, V.G., Nemirovsky, M.S., Udodov, A.I., 1987. Winter convection in the Adriatic and formation of deep eastern Mediterranean waters. *Ann. Geophys.* 5B, 89–92.
- Ozsoy, E., Hecht, A., Unluata, U., 1989. Circulation and hydrography of the Levantine Basin. *Results of POEM Coordinated Experiments 1985–1986. Prog. Oceanogr.* 22, 125–170.
- Pacanowski, R.C., Dixon, K., Rosati, A., 1991. README file for GFDL MOM 1.0. GFDL-NOAA, Princeton, NJ.
- Payne, R.E., 1972. Albedo of the sea surface. *J. Atmos. Sci.* 29, 959–970.
- Peixoto, J., De Almeida, M., Rosen, R., Salstein, D., 1982. Atmospheric moisture transport and the water balance of the Mediterranean Sea. *Water Resour. Res.* 18, 83–90.
- Philander, S.G.H., Hurlin, W.J., Siegel, A.D., 1987. Simulation of the seasonal cycle of tropical Pacific Ocean. *J. Phys. Oceanogr.* 17, 1986–2002.
- Pinardi, N., Korres, G., Lascaratos, A., Roussenov, V., Stanev, E., 1997. Numerical simulation of the interannual variability of the Mediterranean Sea upper ocean circulation. *Geophys. Res. Lett.* 24 (4), 425–428.
- Reed, R.K., 1975. An evaluation of formulas for estimating clear-sky insolation over the ocean. *NOAA Tech. Rep. ERL 352-PMEL*, Vol. 26, 25 pp.
- Reed, R.K., 1977. On estimating insolation over the ocean. *J. Phys. Oceanogr.* 17, 854–871.
- Reed, R.K., Halpern, D., 1975. Insolation and net long-wave radiation off the Oregon coast. *J. Geophys. Res.* 80, 839–844.
- Reynolds R.W., 1982. A monthly averaged climatology of sea surface temperatures. *NOAA Tech. Rep. NWS 31*, Washington, DC, 33 pp.
- Reynolds, R.W., 1988. A real-time global sea surface temperature analysis. *J. Climate* 1, 75–86.

- Robinson, A.R., Golnaraghi, M., Leslie, W.G., Artegiani, A., Hecht, A., Lazzoni, E., Michelato, A., Sansone, E., Theocharis, A., Unluata, U., 1991. The Eastern Mediterranean general circulation: features, structure and variability. *Dyn. Atmos. Oceans* 15, 215–240.
- Rohling, E.J., Bryden, H.L., 1992. Man-induced salinity and temperature increases in the western Mediterranean deep water. *J. Geophys. Res.* 97, 11191–11198.
- Rosati, A., Miyakoda, K., 1988. A general circulation model for upper ocean simulation. *J. Phys. Oceanogr.* 18 (11), 1601–1626.
- Roussenov, V., Stanev, E., Artale, V., Pinardi, N., 1995. A seasonal model of the Mediterranean Sea. *J. Geophys. Res.* 100, 13515–13538.
- Santoleri, R., Bohm, E., Schiano, M.E., 1994. The sea surface temperature of the Western Mediterranean Sea: historical satellite thermal data. In: La Violette, P.E. (Ed.), *Seasonal and Interannual Variability of the Western Mediterranean Sea. Coastal and Estuarine Studies*, Vol. 46, AGU.
- Schiano, M.E., 1996. Insolation over the western Mediterranean Sea: a comparison of direct measurements and Reed's formula. *J. Geophys. Res.* 101 (C2), 3831–3838.
- Schiano, M.E., Santoleri, R., Bignami, F., Leonardi, R.M., Marullo, S., Bohm, E., 1993. Air–sea interaction measurements in the west Mediterranean Sea during the Tyrrhenian Eddy Multi-Platform Observation Experiment. *J. Geophys. Res.* 98, 2461–2474.
- Schlitzer, R., Roether, W., Oster, H., Junghans, H.G., Hausmann, M., Johannsen, H., Michelato, A., 1991. Chlorofluoromethane and oxygen in the Eastern Mediterranean. *Deep-Sea Res.* 38, 1531–1551.
- Schott, F., Visbeck, M., Send, U., 1993. Open-ocean deep convection, Mediterranean and Greenland Seas. In: Malanotte Rizzoli, P., Robinson, A. (Eds.), *Ocean Processes on Climate Dynamics*. Kluwer, pp. 203–225.
- Seckel, G.R., Beaudry, F.H., 1973. The radiation from sun and sky over the North Pacific Ocean. *Trans. Am. Geophys. Union* 54, 1114, Abstract.
- Simpson, J.J., Paulson, C.A., 1979. Mid-ocean observations of atmospheric radiation. *Q. J. R. Meteorol. Soc.* 105, 487–502.
- Slutz, R.J., Lubker, S.J., Hiscox, J.D., Woodruff, S.D., Jenne, R.L., Joseph, D.H., Steurer P.M., Elms, J.D., 1985. COADS, Comprehensive Ocean–Atmosphere Data Set, Release 1. Available in Climate Research Program, ERL, Boulder, CO.
- Smith, S.D., 1989. Water vapor flux at the sea surface. *Boundary-Layer Meteorol.* 47, 277–293.
- Trenberth, K.E., Olson, J.G., 1988. Evaluation of NMC global analyses: 1979–1987. NCAR Tech. Note NCAR/TN-299+STR.
- Trenberth, K.E., Olson, J.G., 1988b. Evaluation and intercomparison of global analyses from the National Meteorological center and the European Centre for Medium Range Weather Forecasts. *Bull. Am. Meteorol. Soc.* 69 (9), 1047–1057.
- Trenberth, K.E., Christy, J.R., Olson, J.G., 1987. Global atmospheric mass, surface pressure, and water vapor variations. *J. Geophys. Res.* 92, 14815–14826.
- U.S. Navy, 1955. *Marine climatic atlas of the world*, Vol. 1. North Atlantic Ocean, Washington, DC.
- Weare, B.C., Strub, P.T., Samuel, M.D., 1981. Annual mean surface heat fluxes in the Tropical Pacific Ocean. *J. Phys. Oceanogr.* 11, 705–717.
- Zavatarelli, M., Mellor, G.L., 1995. A numerical study of the Mediterranean sea circulation. *J. Phys. Oceanogr.* 25 (6), 1384–1414.